Journal of
Nanotheranostics

MDPI

Review

Self-Assembled Monolayers Derived from Positively Charged Adsorbates on Plasmonic Substrates for MicroRNA Delivery: A Review

Johnson Hoang [1], Pooria Tajalli [2], Mina Omidiyan [2], Maria D. Marquez [2], Orawan Khantamat [3], Wirote Tuntiwechapikul [3], Chien-Hung Li [4], Arati Kohlhatkar [2], Hung-Vu Tran [2], Preethi H. Gunaratne [1,*] and T. Randall Lee [2,*]

1 Department of Biology and Biochemistry, University of Houston, Houston, TX 77204-5001, USA
2 Department of Chemistry, The Texas Center for Superconductivity, University of Houston, Houston, TX 77204-5003, USA
3 Department of Biochemistry, Faculty of Medicine, Chiang Mai University, Chiang Mai 50200, Thailand
4 Department of Medicinal and Applied Chemistry, Kaohsiung Medical University, Kaohsiung 807, Taiwan
* Correspondence: phgunaratne@uh.edu (P.H.G.); trlee@uh.edu (T.R.L.)

Abstract: MicroRNA (miRNA) has emerged as a promising alternative therapeutic treatment for cancer, but its delivery has been hindered by low cellular uptake and degradation during circulation. In this review, we discuss the various methods of delivering miRNA, including viral and non-viral delivery systems such as liposomes and nanoparticles. We also examine the use of nanoparticles for miRNA-based diagnostics. We focus specifically on non-viral delivery systems utilizing coinage metals in the form of nanoparticles and the use of self-assembled monolayers (SAMs) as a method of surface modification. We review the use of SAMs for the conjugation and delivery of small noncoding ribonucleic acid (ncRNA), particularly SAMs derived from positively charged adsorbates to generate charged surfaces that can interact electrostatically with negatively charged miRNA. We also discuss the effects of the cellular uptake of gold and other plasmonic nanoparticles, as well as the challenges associated with the degradation of oligonucleotides. Our review highlights the potential of SAM-based systems as versatile and robust tools for delivering miRNA and other RNAs *in vitro* and *in vivo* and the need for further research to address the challenges associated with miRNA delivery and diagnostics.

Keywords: microRNA; miRNA delivery; non-viral delivery systems; plasmonic nanoparticles; self-assembled monolayers; SAMs; miRNA diagnostics; therapeutics; nanotheranostics

Citation: Hoang, J.; Tajalli, P.; Omidiyan, M.; Marquez, M.D.; Khantamat, O.; Tuntiwechapikul, W.; Li, C.-H.; Kohlhatkar, A.; Tran, H.-V.; Gunaratne, P.H.; et al. Self-Assembled Monolayers Derived from Positively Charged Adsorbates on Plasmonic Substrates for MicroRNA Delivery: A Review. *J. Nanotheranostics* **2023**, *4*, 171–200. https://doi.org/10.3390/jnt4020009

Academic Editor: Seyed Moein Moghimi

Received: 21 March 2023
Revised: 23 April 2023
Accepted: 25 April 2023
Published: 8 May 2023

1. Introduction

The use of microRNA (miRNA) to resensitize apoptosis-resistant cancer cells has emerged as a prominent alternative therapeutic treatment to chemotherapeutic drugs [1–5]. Nonetheless, the unfavorably low cellular uptake and degradation during passive circulation have hampered the delivery of miRNA *in vivo* and *in vitro* [6]. The two most notable categories of gene carrier systems to date are viral and non-viral. Viral carriers (retroviruses, lentiviruses, and adenoviruses) offer the advantage of a relatively high transfection efficiency but are hindered due to their immunogenicity and complex preparation methods [7]. Alternatively, non-viral delivery systems (liposomes and nanoparticles) have emerged as contenders for the difficult-to-prepare viral systems. Commercially available, non-viral liposomal delivery systems have therefore emerged at the forefront of therapeutics due to their high cellular membrane affinity, non-immunogenic response, and ease of production. However, these methods still suffer from low transfection efficiency and high cytotoxicity, compared to viral carriers [8]. Furthermore, the emergence of a subclass of non-viral delivery carriers utilizing coinage metals as a platform, in the form of nanoparticles, offers the

advantages of low toxicity and high payload delivery. However, the nanoparticle surface requires modification by adsorbates to impart specific properties [9].

The use of self-assembled monolayers (SAMs) has become a prominent method for surface modification due to the ease of formation via the binding of an adsorbate on a variety of different coinage metals (gold, silver, platinum, and palladium) and the robustness offered to the material by tailoring the interfacial properties of the films [10–14]. The most highly studied substrate for biological applications is gold due to its inert and biocompatible properties [10,15,16]. The adsorbate is composed of a headgroup (i.e., thiol [15–17], silane [18], imidazole [12], or phosphonate [19]) which can be adapted to bind to specific substrates. For gold and related noble metal substrates, thiol headgroups are typically used [13,16,20]. The second component of the adsorbate is a spacer, composed of an alkyl chain that dictates the packing of the resulting films through van der Waals (vdW) interactions [21]. The last major component of the adsorbate is a terminal group. To further tailor SAMs for biological applications, the adsorbate's terminal group can be tailored for biomolecule conjugation; common tailgroups used for these types of applications include ammonium [22], carboxylic acids [23], and thiols [24].

This article provides a review of SAMs that can be used for the conjugation and delivery of small noncoding RNA (ncRNA), particularly SAMs derived from positively charged adsorbates to generate charged surfaces to interact electrostatically with negatively charged miRNA [25]. A brief discussion of the biogenesis and homeostasis of miRNA is given, followed by a discussion of the effects of the cellular uptake of gold and other plasmonic nanoparticles through endocytosis. The final section presents a report on various adsorbate terminal groups used for the conjugation and delivery of oligonucleotides.

2. Roles of miRNA in Gene Regulation

The miRNAs are ~22 nucleotides (nt) small ncRNAs that have a functional role as post-transcriptional regulators of protein-coding genes [26]. In humans, there are more than 2300 miRNAs that are estimated to regulate over 60% of protein-coding genes [26,27]. To understand the role of miRNA as post-transcriptional regulators of oncogenes and tumor suppressors for the development of microRNA therapeutics for the treatment of cancer, brief overviews of miRNA biogenesis, RNA-induced silencing complex (RISC) formation, target recognition, and the modes of gene silencing are described below.

2.1. Biogenesis of miRNAs

The miRNA-encoding sequences are found in both intragenic regions and intergenic regions of a genome. The intragenic miRNAs are embedded within a host gene, which can be a protein-coding gene or a noncoding RNA gene. The recent analysis of 1881 miRNAs found that about 76.2% of miRNAs can be classified as intragenic miRNAs, of which the majority resides within an intron of the host gene (48.8% of 1881 miRNAs), while the intergenic miRNAs account for another 23.8% [28].

The biogenesis of intragenic miRNAs can be both host-gene-dependent or independent. The early model suggested the co-expression of both miRNA and the host gene using the same promoter, and miRNAs are processed from the same primary transcripts as their host genes [29,30]. However, a study using genome-wide miRNA and gene expression profiles found that only a fraction of intragenic miRNAs is coexpressed with their host genes [31]. Another study of human genomes using PROmiRNA, a miRNA promoter recognition method, found that up to 62% of miRNAs have their own promoters whose expression occurs independently from their host gene transcriptions [32]. The same PROmiRNA study also found that 83.7% of intergenic miRNAs have at least one promoter [32]. Note that the PROmiRNA study employed data from the deepCAGE database, which gathers information from only 5′-capped transcripts. Therefore, these miRNAs were transcribed by RNA polymerase II. The undetected miRNAs in the study might be the miRNAs transcribed by RNA polymerase III [33,34], or the primary miRNA transcripts were not detectable due

to various reasons [32]. Furthermore, many intergenic miRNAs are located in the same clusters and they could be transcribed under the same promoter [35,36].

The biogenesis of miRNAs has been extensively reviewed elsewhere [26,29,37,38]. Figure 1 summarizes the canonical pathway of miRNA biogenesis. In general, regardless of their location in the genome, most miRNAs are transcribed by RNA polymerase II under their own promoters or the host-gene promoters in the case of some intragenic miRNAs. The primary miRNAs (pri-miRNAs) are usually long, up to several thousand nt in length, with a section of about 60–80 nt that forms a hairpin structure, where the mature miRNA is embedded in the stem [38,39]. In the nucleus, the pri-miRNAs are first bound by a double-stranded RNA-binding protein DiGeorge Syndrome Critical Region 8 (DGCR8) and cleaved by Drosha. Drosha, a class II ribonuclease III enzyme, cleaves the pri-miRNA in the stem near the base of the hairpin structure to generate a miRNA precursor (pre-miRNA) with a 2-nt 3′-overhang [38]. The pre-miRNAs are then exported through the nuclear pore to the cytosol by Exportin-5 (EXP5 or XPO5), which forms a transport complex with Ran-GTP upon binding to a pre-miRNA [38]. Once in the cytoplasm, Ran-GTP is hydrolyzed to Ran-GDP, and the transport complex is disassembled, releasing pre-miRNA [38]. The pre-miRNA is then processed into a mature miRNA by Dicer, an RNase III endoribonuclease, in association with a double-stranded RNA binding protein trans-activation response (TAR) RNA-binding protein (TRBP) [38,40]. Dicer recognizes the 2-nt 3′-overhang of the pri-miRNA by its Platform-PAZ-connector (PPC) domain, and the two RNase III domains cleave the dsRNAs stem of the hairpin ~22 nt from the 3′-end, generating a mature miRNA duplex with the two distinct characters, a monophosphate group at the 5′-end and a 2-nt 3′-overhang, on both ends [41].

2.2. RNA-Induced Silencing Complex (RISC) Formation

The Dicer-TRBP complex, together with the mature miRNA duplex, interacts with an Argonaute (AGO) protein to form the RISC-loading complex (RLC) [40]. The miRNA duplex is then unwound; one strand (guide strand) remains with the RLC, while another strand (passenger strand) is sometimes discarded and subsequently degraded [37]. In some fractions of the miRNAs, both strands act as guide RNAs for different mRNA targets. Any RNA strand of the miRNA duplex can remain in the RLC and, therefore, act as miRNA in the RISC. However, the preference for one strand over another varies widely depending on cell type, cellular environment, and the type of nucleotide at the 5′-end [37].

Once the selection of the miRNA's guide strand is completed, the RLC is allowed to form the RNA-induced silencing complex (RISC) [42,43]. RISC is a generic term for ribonucleoprotein complexes that repress the expression of target genes at the transcriptional or post-transcriptional levels [41]. An RISC is comprised of a small RNA and a member of an AGO protein family, along with the set of effector proteins recruited by each specific AGO [41].

The small RNAs in an RISC are generally classified into three groups: miRNAs, small interfering RNAs (siRNAs), and P-element-induced wimpy testis (PIWI)-interacting RNAs (piRNAs) [44]. These RNAs are classified as small noncoding RNAs (sncRNAs), which are distinguished from long noncoding RNAs (lncRNAs) based on their size at 200 nucleotides. The miRNAs and piRNAs are transcribed from genomic DNA. However, the siRNAs are synthetic double-stranded RNAs introduced into cells with the purpose of targeting a specific mRNA for degradation [44]. Much like the miRNAs mentioned above, the cellular-introduced double-stranded RNAs are processed by Dicer to generate siRNAs, double-stranded RNAs typically 20–24 base pairs in length, which then guide and align the RISC on the target mRNA [43]. Another form of RNA interference that mimics both miRNA and siRNA is the short hairpin RNA (shRNA). Instead of introducing the cells with a double-stranded RNA to produce siRNA, the siRNA sequence is embedded in an artificial gene with an RNA polymerase II/III promoter. The gene is then delivered into the cells in the form of a plasmid or with a viral vector. After transcription by RNA polymerase, the primary transcript forms a short hairpin structure that is processed to

shRNA by the Drosha-DGCR8 complex and follows the miRNA biogenesis pathway to form the RISC [45]. The last group of small RNA in RISC is piRNA. The piRNAs bind the PIWI subfamily of AGO proteins to specific targets of activated transposable elements or retroviral that have invaded our genome and play roles in transposable element repression, gene regulation, and viral defense [46]. They are distinct from miRNA in size (26–31 nt). The biogenesis of piRNAs is independent of Dicer, and their mechanisms remain an active area of research [45].

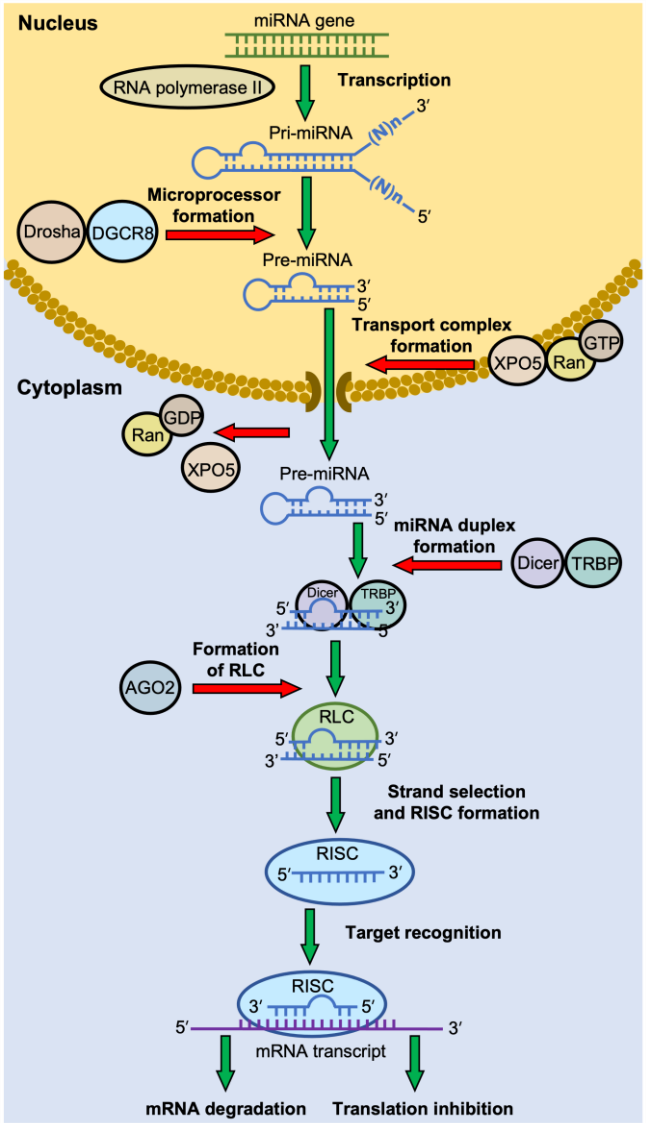

Figure 1. The canonical pathway of miRNA biogenesis. Most miRNA genes are transcribed by RNA polymerase II. The primary miRNAs (pri-miRNAs) are usually long, with a section of ~70 nt that forms a hairpin structure. The pri-miRNAs are cleaved into a miRNA precursor (pre-miRNA) in the nucleus by a microprocessor complex consisting of Drosha and DiGeorge Syndrome Critical Region 8 (DGCR8) protein. The pre-miRNA is then exported to the cytosol by the complex of Exportin-5 (XPO5) and Ran-GTP. In the cytoplasm, Ran-GTP is hydrolyzed to Ran-GDP, and the transport complex releases its pre-miRNA. The pre-miRNA is then cleaved by Dicer, in association with trans-activation response (TAR) RNA-binding protein (TRBP), to generate a mature miRNA duplex. The miRNA duplex-Dicer-TRBP complex then interacts with an Argonaute (AGO) protein to form the RISC-loading complex (RLC). AGO selects a guide strand, and the assembly of the RNA-induced silencing complex (RISC) proceeds. RISC recognizes the mRNA target through base-pairing with the miRNA, which then leads to mRNA degradation or translation inhibition.

Argonaute protein (AGO) is the other essential component of the RISC besides the small RNA [42]. The eukaryotic AGO family is divided into four classes: AGO-like family, PIWI-like family, WAGO family, and Trypanosoma AGO family [47]. Each AGO family has its preference for the group of small RNA and may interact with distinct effector proteins, leading to different functions in gene regulation [42]. There are eight Argonaute proteins in humans: four AGO proteins and four PIWI proteins [47]. The four AGOs share ∼80% amino acid homology and often bind the same set of miRNAs [48]. AGO2 is the most studied because it is the most abundant AGO in many cells, and the AGO2 gene is the only essential gene among the four paralogs [48]. AGO2 was believed to be the only AGO that processes endonuclease activity (slicing activity) until AGO3 was also found to have this activity as well [48].

Nakanishi et al. redefined the AGO structure into six domains from N-terminal to C-terminal as follows: N-domain (N), Linker I (L1), Piwi-Argonaute-Zwille (PAZ), Linker 2 (L2), Mid domain (MID), and P-element-Induced Wimpy (PIWI) [48]. The N-domain unwinds the miRNA duplex during the RISC assembly. The PAZ domain binds the 3′-end of the guide strand, protecting it from RNA degradation and aiding the RISC assembly. The MID domain anchors the 5′-end of the guide strand between the MID-PIWI lobe. The PIWI domain, which contains the catalytic DEDH (Asp-Glu-Asp-His) tetrad in AGO2 and AGO3, is responsible for mRNA cleavage for these AGOs. The L1 and L2 linkers contribute to the overall structural stability of the RISC.

2.3. Target Recognition by RISC

The mature RISCs bind their target mRNAs and silence their expression by initiating mRNA degradation or translational repression, depending on the degree of guide miRNA-mRNA complementarity or the effectors recruited by each AGO protein [42]. Figure 2 illustrates the guide strand in the RISC and its target mRNA (an example from an RISC with the AGO2 protein). Human miRNAs prominently bind their mRNAs in the 3′-untranslated region (3′-UTR) [42]. The guide miRNA strand can be divided into four domains from 5′ to 3′: the seed, central, 3′-supplementary, and tail regions. The seed region, the second nt to eighth nt (g2–g8) from the 5′-end, is essential for target recognition using conventional base pairing. The central region (g9–g12) is important for mRNA and passenger strand cleavage. The 3′-supplementary region (g13–g17) further stabilizes the complex by base pairing with the mRNA target. The tail region (g18-3′ end) affects the turnover of target cleavage, regulates the recruitment of additional factors, and determines the fate of the RISC. After RISC assembly, the 5′ end and 3′ end of the guide miRNA strand are docked into the 5′ and 3′ binding pocket of the AGO protein, respectively. The seed and the supplementary regions are accommodated in the corresponding chambers that are positioned next to each other and bridged by the 1–15 nucleotide loop of target mRNA. The adenine residue at the t1 position of target mRNA (t1A) is interacted with the t1A recognition pocket of the AGO protein which enhances RISC binding [42].

2.4. Modes of Gene Silencing

The modes of gene silencing by the RISC can be divided into mRNA cleavage and translational repression [42]. It is determined primarily by which AGO protein is incorporated into the RISC and, therefore, its associated effector proteins [48]. However, even with the same AGO, the degree of complementarity between the guide strand and the target mRNA can affect the mode of gene silencing [42]. Animal miRNAs often target their mRNAs at the 3′-UTR and translationally repress them. However, plant miRNAs or animal siRNAs, due to the type of AGO protein and the extensive base pairing to their target mRNAs, often degrade their mRNAs [42].

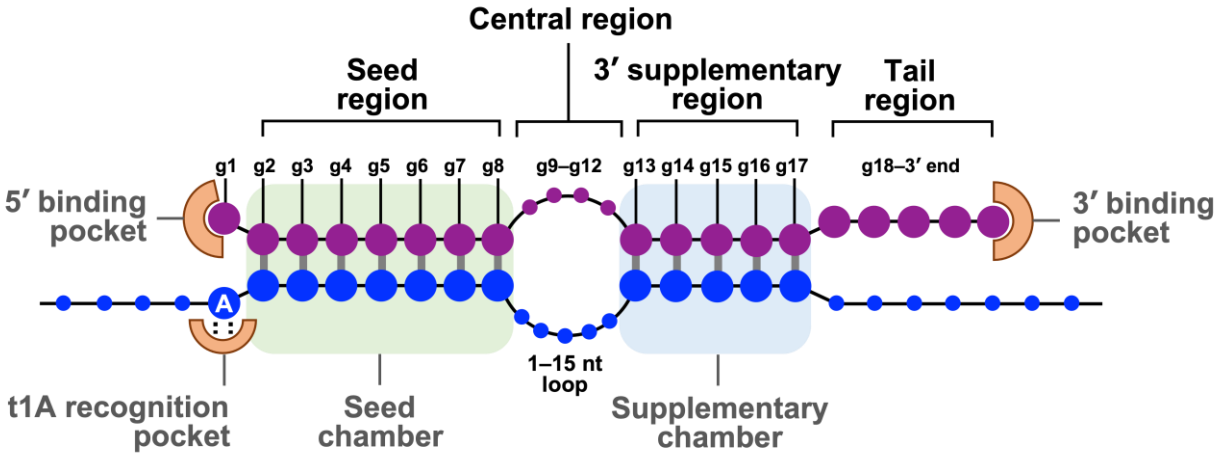

Figure 2. The base pairing of guide strand in RISC and its target mRNA. Schematic represents base pairing between a guide miRNA strand (purple) and a target mRNA (blue). The guide miRNA strand can be divided into four domains from 5′ to 3′. The seed region (g2–g8) is essential for target recognition. The central region (g9–g12) is important for mRNA and passenger strand cleavage. The 3′-supplementary region (g13–g17) stabilizes the complex with the mRNA target. The tail region (g18-3′ end) regulates the turnover of target cleavage and the fate of RISC. The 5′ end and 3′ end of the guide strand are anchored in the MID and PAZ domains of AGO2, respectively. Adapted with permission from reference [42]. Copyright 2022, Cell Press.

In the mRNA cleavage mode, the mature RISC must contain AGO with the slicing activity. As mentioned above, only AGO2 and AGO3 possess this activity in humans [48]. The PIWI domain of AGO2, which has the conserved DEDH catalytic tetrad, forms an RNase H-like fold that cleaves the target mRNA when it is extensively base-pairing with the miRNA by which the g10 and g11 are also paired [48]. However, as shown in Figure 2, this central region often forms a loop with animal RISCs; therefore, mRNA cleavage is not the major mode of gene silencing in animals [42].

The mechanisms of miRNA-mediated translational repression and mRNA decay are complicated and less understood [42]. The widely accepted model is the GW182-dependent mechanism. The GW182 protein, or the human paralog TNRC6, binds AGO proteins in the mature RISC and promotes the dissociation of the poly(A)-binding protein (PABP) from the target mRNA. Since the PABP gets involved in the translation initiation by promoting the closed-loop structure with the 5′-cap via its interaction with eIF4E, dissociating the PABP from the Poly(A) tail disrupts the loop structure; therefore, translation initiation and ribosome recycling are repressed [42]. After translation arrest, RISC-GW182 interacts with the CCR4-NOT complex, a multisubunit deadenylase machinery, which shortens the 3′-Poly(A) tail. The large scaffolding subunit of CCR4-NOT, CNOT1, binds directly to DDX6, the translational repressor and decapping activator protein that stimulates mRNA decapping. Finally, the decapped mRNAs are degraded by the 5′–3′ exonuclease, Xrn1 [49].

3. Role of MicroRNA in Cancer

Due to the small binding requirement (a minimum of six consecutive nucleotides in the 5′-seed of the miRNA must perfectly pair with a sequence in the 3′-UTR of the mRNA target) a single microRNA can bind and silence hundreds of mRNA targets to at once impact multiple pathways [50]. Consequently, the dysregulation of miRNA causes an adverse effect on cellular proliferation and differentiation [50,51]. Studies have shown that miRNA mutations or mis-expression correlate with various human cancers and have the potential to function as tumor suppressors (tumor suppressor miRNA) or as oncogenes (oncogenic miRNA) based on their inhibition of a large variety of oncogenic or tumor-suppressive mRNAs [51–53].

In normal tissues, miRNA is essential for the post-transcriptional regulation of mRNA (Figure 3A) [51]. By binding to target mRNA, it represses target-gene expression through the inhibition of protein translation or altered mRNA stability, allowing for normal rates of cellular division, proliferation, differentiation, and cell death [54]. However, downregulation of tumor suppressor miRNA increases the translation of oncogenes (Figure 3B), resulting in increased proliferation, decreased apoptosis, and tumor formation. The defects at any stage of miRNA biogenesis can cause a decrease in tumor suppressor miRNA. Tumor suppressor miRNAs that have been reported include the Let-7 family: miR-15a, miR-29, miR-31, miR-34, miR-126, miR-145, and miR-203 [52,55]. Conversely, upregulation of oncogenic miRNA blocks the expression of a miRNA-target tumor-suppressor gene and leads to tumor formation (Figure 3C). Increased levels of oncogenic miRNA can result from miRNA gene amplification, a constitutively active promoter, increased efficiency in miRNA processing, or increased miRNA stability. Some examples of oncogenic miRNAs include the miR-17~92 cluster: miR-21, miR-155, miR-221, miR-222, miR-372, and miR-373 [52,55,56].

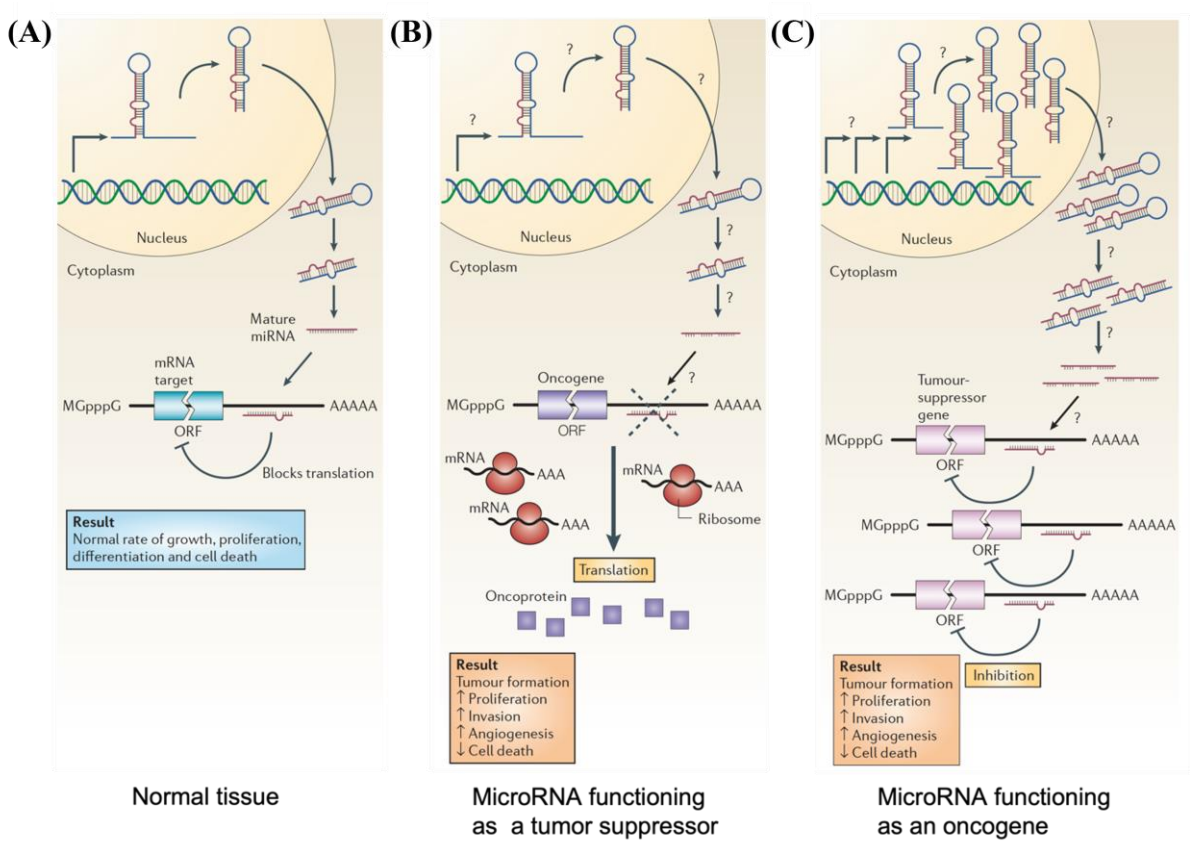

Figure 3. Schematic illustrations depicting (**A**) normal growth, proliferation, differentiation, and cell death in normal tissue occurring through proper microRNA transcription; (**B**) defects at different stages of tumor suppressor miRNA biogenesis leading to the formation of oncoproteins; and (**C**) overexpression of oncogenic miRNA inhibiting expression of tumor suppressor protein and resulting in tumor formation. Reproduced with permission from reference [51]. Copyright 2006, Springer Nature.

Significant advances in understanding miRNA have allowed its use as an alternative therapeutic treatment for cancer [57]. At present, over 30,000 patents in "Google patent" can be found within the United States, demonstrating the importance of miRNA research and its regulatory factors in therapeutically treating cancer [57]. As an imbalance in miRNA expression levels is associated with tumorigenesis, there are two major approaches to developing miRNA-based cancer therapies: miRNA replacement and miRNA inhibition [53,58,59]. miRNA replacement involves using miRNA mimics to enhance the function of endogenous miRNAs and restore the expression of tumor suppressor miRNAs [52,53]. On the other

hand, miRNA inhibition refers to the use of miRNA antagonists (anti-miRNAs), single-stranded antisense oligonucleotides designed to silence overexpressed oncogenic miRNAs in cancer cells [52,53]. These miRNA mimics and anti-miRNAs can be delivered into tumor cells either via a viral or non-viral (chemical and physical approach) delivery system [57]. In the following sections, the various methods of delivering miRNA, including viral and non-viral delivery systems such as liposomes and nanoparticles, and the effects of the cellular uptake of the plasmonic nanoparticles through endocytosis are discussed.

4. Endocytosis of Gold Nanoparticles

4.1. Gold Nanoparticles Entering the Lysosome

Rapid advances in the field of the intracellular uptake of nanocarriers still require more studies to overcome the obstacles of solubility, non-specific binding, poor bioactivity, and toxicity [60]. The results require further development toward safe passage into the cytoplasm of the cellular compartment by these carriers. Fine tuning the nanocarriers for applications is highly dependent upon their physical attributes—such as size, shape, and interfacial properties—which play a significant role in their passage into cells, which in turn affects circulation, cellular uptake, and efficacy [61–63]. The internalization of particles can occur through two different methods: non-ligand and ligand assistive internalization into cells [64].

The cellular internalization efficiency and uptake pathway of gold nanoparticles is dependent on the particle's charged chemical composition [64]. The charge component of the particle can lead to numerous interactions with various biomolecules within a system, affecting the internalization of the particles [64]. Positively charged gold nanoparticles have been demonstrated to be internalized more rapidly and more efficiently than negatively charged or neutral species [65]. Additionally, the size and shape of the nanoparticles also affect cellular internalization efficiency [63]. For example, Noël et al. conducted a study using TEM to evaluate the internalization of gold nanoparticles with sizes of 70 nm and 20 nm in polymorphonuclear neutrophil cells (PMNs). They found that 70 nm sized gold nanoparticles were unable to pass the cell membrane, while 20 nm sized nanoparticles were not restricted by the cell membranes after treating PMNs with particles for 1 h [66]. The notable work performed by Chithrani et al. compared the cellular uptake of spherical gold nanoparticles as a function of size (14, 30, 50, 74, and 100 nm) [67]. The study determined that the greatest amount of spherical gold nanoparticles that internalized into cells were 50 nm in size, with an intake rate of 1294 nanoparticles per hour. The internalization of the nanoparticles is likely due to the desorption of the citrate-stabilizing agent by the nonspecific adsorption of serum proteins (e.g., Alpha and Beta globulin proteins) through the receptor-mediated endocytosis pathway. Furthermore, a comparison between the spherical 74 nm and 14 nm nanoparticles and the 74 nm × 14 nm gold nanorods showed that the spherical gold nanoparticles were endocytosed more efficiently than the nanorod gold nanoparticles. The authors speculated that the longitudinal axis of the nanorod may encompass more receptors, which hinders the number of sites for further binding. The authors also concluded that the ligand may not have been fully displaced by citrate, consequently causing the proteins to inefficiently bind to the surface of the nanoparticles.

Follow-up studies performed by Nambara et al. demonstrated that gold nanoparticles with triangular morphology exhibited a 20-fold higher level of cellular uptake into HeLa cells compared to spherical particles with a similar surface area [68]. Furthermore, Xie et al. evaluated the cellular uptake of the 50 nm nanoparticles using different shapes such as stars, rods, and triangles [69], all of which utilized the clathrin-mediated endocytosis pathway for cellular uptake. The order of preference for cellular uptake was triangles > rods > stars. Upon analyzing the findings, the authors determined that the preference of the internalization of different shapes is dependent upon membrane-bending energy to internalize the nanoparticles.

The impact of shape, size, and charge are crucial for gene carrier design and the cellular uptake of nanoparticles. Nanoparticles conjugated with small interfering RNA

(siRNA) have been shown to be impacted by these attributes (shape, size, and charge) during cellular uptake [61]. In their assessment, Yue et al. determined that the cellular uptake of a 50 nm spherical nanoparticle had a higher uptake compared to a smaller 13 nm spherical nanoparticle [61]. The authors also compared 50 nm spherical nanoparticles with 40 nm star-shaped nanoparticles and determined that the cellular uptake was greater for the former. It was observed that the localization of the nanoparticles occurred within two hours of incubation with the cells. At 24 h, the 50 nm and 40 nm sized nanoparticles were not present in the endosome or lysosome but rather formed aggregations within the cytoplasm. In contrast, the 13 nm nanoparticles were found to still be present within the endosomal and lysosomal compartments, without aggregation.

4.2. Gold Nanoparticles Exiting the Lysosome

To successfully delivery therapeutic agents, such as oligonucleotides, with nanoparticles, the therapeutic device must overcome intracellular and intercellular barriers to effectively deliver unmodified agents. To achieve successful transfection, measures must be taken to ensure the sequestering of the negatively charged phosphate backbone and hydrophobic framework of the oligonucleotide. However, oligonucleotides must elude enzymatic degradation before and after delivery into the cytoplasm [70]. Once in the cytoplasm, endosomal escape must occur for oligonucleotides to effectively interact with mRNA. The most prominently proposed mechanism for the escape of inorganic nanoparticles is endosomal escape through the "proton sponge" effect (Figure 4) and the formation of ion pairs [71–73].

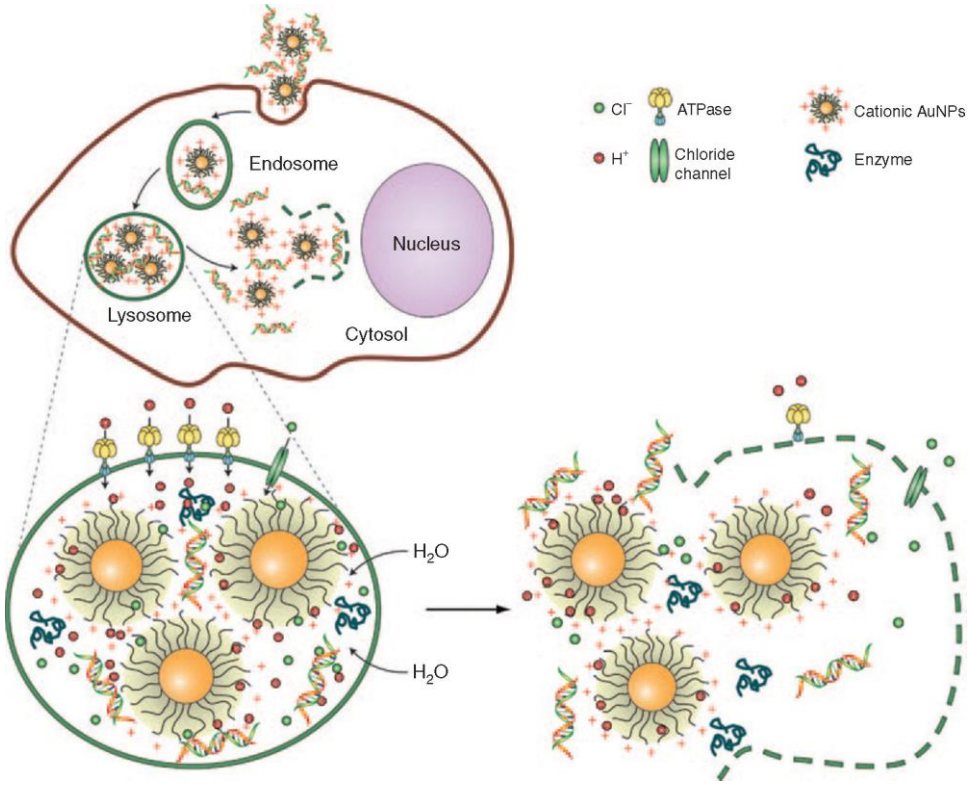

Figure 4. Depiction of the "proton sponge" mechanism after endocytosis of gold nanoparticles to escape the endosome. Reproduced with permission from reference [74]. Copyright 2009, Springer Nature.

Typically, proton sponge effects are observed prominently in amine nanocomplex systems [74]. After the internalization of the nanocomplex into the cell, the cumbersome mechanical task of escaping endosomal and lysosomal degradation is crucial. During this process of acidification to initiate degradation, the ATPase proton pump decreases

the pH inside the cells, causing the translocation of protons into the endosomes. The cationic nanocomplex group becomes protonated and subsequently activates hydrolytic enzymes [74–77]. The continuous flow of protons and chloride ions into the endosome causes an influx of water, which results in high osmotic pressure and the rupture of endosomes, releasing the contents into the cell's cytoplasm [74–77].

The proposed mechanism of forming ion pairs to escape lysosomes offers an alternative approach to the proton sponge effect [73]. Utilizing the anionic species of the lysosomal membrane, the AuNPs can be functionalized with a cationic species to disrupt the lipid membrane, which facilitates endosomal escape into the cytoplasm [73].

5. Using SAMs to Modify the Surfaces of Gold and Other Plasmonic Nanoparticles

Self-assembled monolayers are essential in increasing the stability, dispensability, and conjugation of oligonucleotides on the nanoparticle surface [78]. SAMs are composed of three essential components (Figure 5): the terminal functional group, which can be tailored to tune the dispersibility of the particles in the solvent of choice or, more importantly, for the conjugation of oligonucleotides; the spacer group, which provides stability to the film through vdW interactions; and the headgroup, which can be manipulated to bind onto a variety of substrates [79,80].

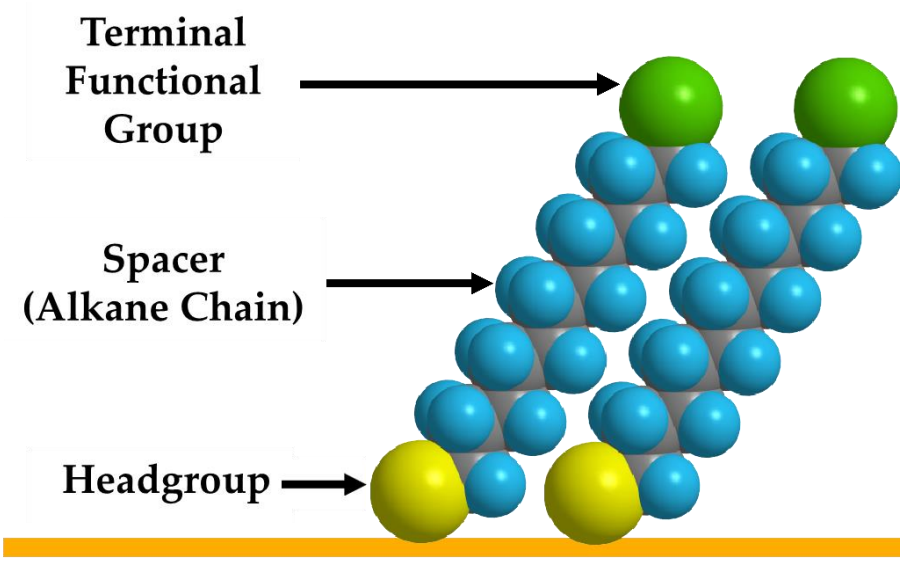

Figure 5. Schematic representation of the three essential parts of the adsorbate (terminal functional group, spacer, and headgroup on the substrate).

Due to its biological compatibility and inertness, gold is the most notable substrate used as a platform for developing drug delivery systems [81,82]. Furthermore, this extensively explored substrate can be modified with SAMs composed of a thiol headgroup [83]. The most extensively studied headgroups are thiols, due to their high affinity to gold, ~40 kcal/mol [84]. Immobilization of the thiol-based SAMs to the gold nanoparticle substrate can be achieved through the chemisorption of the adsorbates by the ligand exchange of stabilizing agents present on the gold nanoparticles [85,86]. However, this method is more challenging than forming SAMs on flat coinage metal substrates, which require simple incubation of the substrate in a thiol-based adsorbate solution, due to the need for optimizing the incubation parameters to ensure adequate surface coverage and inhibit nanoparticle aggregation [85,86]. Alternatively, a "one-pot" reaction can be used where the thiol adsorbate can serve as a stabilizing surfactant during gold nanoparticle synthesis [83]. On the other hand, it should be noted that other plasmonic metals such as silver (Ag) [87], palladium (Pd) [88], and platinum (Pt) [89] can also be used as substrates in SAMs. Additionally, intracellular biothiols can cleave the Au-S bond and increase the

background signals in cell imaging. Using Pt as a coating on AuNPs can improve the stability of thiolated SAMs as the Pt-S bond is more stable than the Au-S bond [89].

Huang and co-workers demonstrated that there was a direct correlation between the inertness of gold nanoparticles, the aggregation of nanoparticles, and dispersion within the medium, which highlights the necessity of the stabilization of the gold nanoparticles within the system [90]. The tendency of gold nanoparticles to aggregate stems from Van der Waals forces [91]. Tailoring SAMs to include a charged terminal group or to create steric effects can prevent aggregation of the nanoparticles [92]. Ren and co-workers performed a stability study using a series of adsorbates to study chemical stability and dispersity. The adsorbates included polyethylene glycol (PEG-SH), glutathione, mercaptopropionic acid (MPA), cystamine, and dihydrolipoic acid [93]. In this study, the authors analyzed the chemical stability and dispersibility of the adsorbate-functionalized AuNPs in an aqueous system with a pH buffer of 5.4–9.4 and a sodium chloride (NaCl) concentration of 0.005–0.08 M [93]. They showed that PEG-SH was the most stable in a variety of pH values, compared to the other adsorbates; the polymer coating of PEG-SH on gold formed a sterically hindered gold nanoparticle resulting in stable dispersion. Furthermore, the combination of MPA with PEG-SH demonstrated the capability to stabilize and to conjugate epidermal growth factor receptor (EGFR) antibodies onto the gold nanoparticle, thus enabling its use as an imaging agent.

6. Plasmonic Nanoparticles for miRNA Delivery/Detection

Nanoparticles for miRNA Delivery

RNA interference (RNAi) is a type of endogenous gene silencing that occurs after transcription; RNAi acts as a regulatory mechanism that utilizes double-stranded RNA to target mRNA for degradation and silence genes, and it has been widely applied to the study of gene cellular function [94]. MicroRNAs (miRNAs) and small interfering RNAs (siRNAs) are the most well-known molecules [94]. Due to their unique characteristics and advantages over DNA-based therapies, they have emerged as a potential future medicine [94,95]. miRNAs have a greater therapeutic application than siRNAs due to the fact that miRNA recognition requires binding to a significantly shorter seed sequence (two to eight nucleotides) than the entire nucleotide sequence of siRNA [96]. MicroRNA-based therapeutics have been investigated for the treatment of a variety of diseases such as cardiovascular pathologies, diabetes, cancer, and neuroinflammation [97]. As a result, the ability to control the expression of in vivo miRNA will serve as the foundation for treatment development. Two approaches are commonly used for miRNA-based therapeutics: miRNA inhibition and miRNA replacement [98]. When the miRNA of interest is overexpressed, inhibition is used. This objective has been pursued by using the synthetic single-stranded RNAs (called miRNA antagonists) or mRNAs with multiple target sites for a specific miRNA (called miRNA sponges) that are partially or fully complementary to the target miRNA and act as miRNA antagonists (anti-miRNA) by inhibiting the binding to endogenous mRNA targets [99]. When the target miRNA is downregulated, however, miRNA mimics (replacement therapy) are utilized [99]. Small synthetic double-stranded molecules can be converted into functional miRNA or miRNA expression vectors in order to induce miRNA expression in cells and deliver miRNA [99]. Synthetic double-stranded miRNAs mimic the function of target miRNAs and bind to their target mRNA to repress gene expression post-transcriptionally [99].

As with other nucleic acid therapeutics, the lack of an efficient delivery system is the primary obstacle preventing the implementation of miRNA-based therapies in clinical practice [95]. Developing efficient nucleic acid delivery systems to target cells with low toxicity and high bioavailability is therefore a significant challenge for gene therapy [95]. Utilizing microRNAs and nanotechnology to develop clinically viable treatment options is a promising strategy [95]. There are two types of vectors for gene delivery: (a) viral carriers, in which genetic material is integrated into a virus, and (b) non-viral carriers, such as cationic molecular carriers such as lipids and polymers that can form electrostatic

interactions with nucleic acids to deliver genes to cells [95]. Due to their high transfection efficiency, viral vectors are used in the majority of gene therapy applications [100]. The immunogenicity and mutagenicity of viral vector delivery systems, on the other hand, may limit their clinical application [101]. These limitations led to the development of non-viral gene carriers (lipid-based NPs, polymer-based carriers, and inorganic NPs). Non-viral vectors are less immunogenic, less expensive, and more versatile than viral vectors. These carriers can hold large nucleic acids and can be functionalized with specific ligands to target organs or cells [102]. Recently, the use of plasmonic nanoparticles, particularly gold nanoparticles (AuNPs), as non-viral gene delivery vectors, has received attention due to their unique physicochemical properties, which include a range of sizes, morphologies, chemical and thermal stability, a high surface-to-volume ratio, strong localized surface plasmon resonance (LSPR), high biocompatibility, and low immunogenicity [103]. It is worth mentioning that some properties such as size, shape, and surface charge can affect AuNP cytotoxicity [65]. For instance, studies have shown that AuNPs with a diameter of 5 nm can disrupt the cytoskeletal organization of fibroblasts [95]. Additionally, fiber-shaped nanoparticles have been found to be more toxic compared to spherical nanoparticles [65]. Furthermore, charged nanoparticles have shown to have higher cytotoxicity than neutral ones [65]. Various strategies can be used for nucleic acid incorporation depending on the nature of the material core: encapsulation within the material matrix, adsorption with materials containing cationic moieties, or covalent attachment when the NP surface can be modulated by reactive groups. Gold nanoparticles can be easily functionalized with thiol or amino groups to allow electrostatic surface loading of negatively charged miRNAs [104,105]. Selected nanoparticle systems used for miRNA delivery are summarized in Table 1.

To enhance their therapeutic applications, anti-miRs and miRNA mimics have been chemically modified to improve their stability and biodistribution properties [106]. Hao et al. synthesized and characterized novel miRNA-Au nanoparticles that mimic native miRNA [106]. They designed two AuNP-miRNA conjugates to target the mRNA of PRKC and PTEN/E2F1 using miR-205 and miR-20a, respectively [106]. Nanoparticles carrying mimics of the tumor-suppressive miR-205 inhibit the expression of the miR205 target protein by interacting with the 3′ untranslated region of the target mRNA [106]. Based on phenotypic assays, these conjugates inhibit cancer cell proliferation and migration. Nanoparticles mimicking oncogenic miR-20a promote cell survival by downregulating target proteins [106]. These polyvalent nucleic acid-functionalized nanoparticles can enter cells without cationic lipids and polymers, and their function as endogenous miRNAs makes them important new candidates for miRNA replacement therapies and promising new tools for studying miRNA function [106].

Table 1. Nanoparticles for miRNA Delivery.

Plasmonic Substrate	Morphology	Delivery Approach	Size (nm)	Conjugate	Target miRNA	Target Cell	Ref.
Au	Nanosphere (AuNPs)	miRNA inhibition	2.6	Terminated PAMAM	miR-21i	Cancer cells	[107]
		miRNA inhibition	5	Carrier DNA	Anti-miRNA-712	Endothelial cells	[108]
		miRNA inhibition	10	Streptavidin	miRNA-491	Breast cancer cells	[109]
		miRNA inhibition	13	Thiol-modified miRNA	miRNA-182	GBM cells	[110]
		miRNA inhibition	13	Cargo DNA	MiR-29b	Myeloid cells	[111]
		miRNA inhibition	20	Thiolated miRNA	MiR-214	HEK293 cells	[112]

Table 1. *Cont.*

Plasmonic Substrate	Morphology	Delivery Approach	Size (nm)	Conjugate	Target miRNA	Target Cell	Ref.
		miRNA replacement	20	SH-PEG-NH_2	miRNA-206	Breast cancer cells	[103]
		miRNA replacement	13	Thiol-modified RNA	miRNA-205 and miRNA-20a	Prostate cancer cells	[106]
		miRNA replacement	13	Thiolated miRNA	MiRNA-130b	Myeloma cells	[113]
		miRNA replacement	14	Cysteamine	miRNA-31 and miRNA-1323	Neuroblastoma cells and ovarian cancer cells	[114]
	Hollow sphere	miRNA inhibition	61	Thiolated PAMAM	Anti-miR-21i	GBM cells	[115]
		miRNA inhibition	150	Thiolated miRNA	miRNA-34a	TNBC cells	[116]
		miRNA inhibition	30, 50, and 70	SH-PEG-OMe	miRNA-26a	Cancer cells	[117]
	Nanocage	miRNA inhibition	50	Cationic polyethylene-imine	anti-miR-181b	HCC cells	[118]
		miRNA replacement	50	Polyethylene-imine	miR-122	HCC cells	[119]
Au-iron oxide	Nanostar	miRNA inhibition	15	β-cyclodextrin-chitosan hybrid polymers	AntimiR-21 and miR-100	GBM cells	[120]
Au@Bi_2Se_3	Sphere	miRNA inhibition	11	Thiol-modified ssDNA	antagomiRNA-152	Neuroblastoma cells	[121]

Crew et al. investigated miRNA-130b immobilized on AuNPs for cell transfection (see Figure 6) [113]. Thiolated miRNA formed a disulfide bond with AuNPs (Figure 6A). The addition of oligoethylene glycol thiol stabilized the particle surface by preventing RNA from folding and binding electrostatically (Figure 6B). The transfection of multiple myeloma cells with the miRNA-AuNPs revealed an efficient knockdown in a functional luciferase assay (Figure 6C) [113]. It is remarkable that 4% miRNA coverage on the nanoparticles could give rise to such a high knockdown efficiency in the functional luciferase assay [113].

Using gold nanocages, Huang et al. combined anti-miR-181b and photothermal therapies (PTT) [118]. AntimiR-181b encapsulated on PEI-modified, folate receptor (FR)-targeted, and PEG-coated gold nanocages (AuNCs) facilitated cellular uptake and reduced hepatocellular carcinoma (HCC) cell viability [118]. The combination of AuNC-mediated delivery of anti-miR-181b and laser irradiation inhibited tumor growth and induced apoptosis in nude mice bearing HCC tumors [118]. In a similar study, AuNCs were designed to co-deliver doxorubicin (DOX) and miR-122 mimic with PTT for the treatment of HCC [119]. Polyethyleneimine (PEI) was added to AuNCs loaded with 11-mercaptoundecanoic acid (MUA) and DOX for miRNA attachment [119]. PEG and hyaluronic acid (HA) were conjugated with nanocarriers to improve stability and targeting [119]. This method effectively delivered DOX and miR-122 in vitro and in vivo. In a nude mouse model of HCC, this modified AuNC–DOX/miR-122 multifunctional delivery system had a superior antitumor effect compared to any single treatment without causing significant organ toxicity [119].

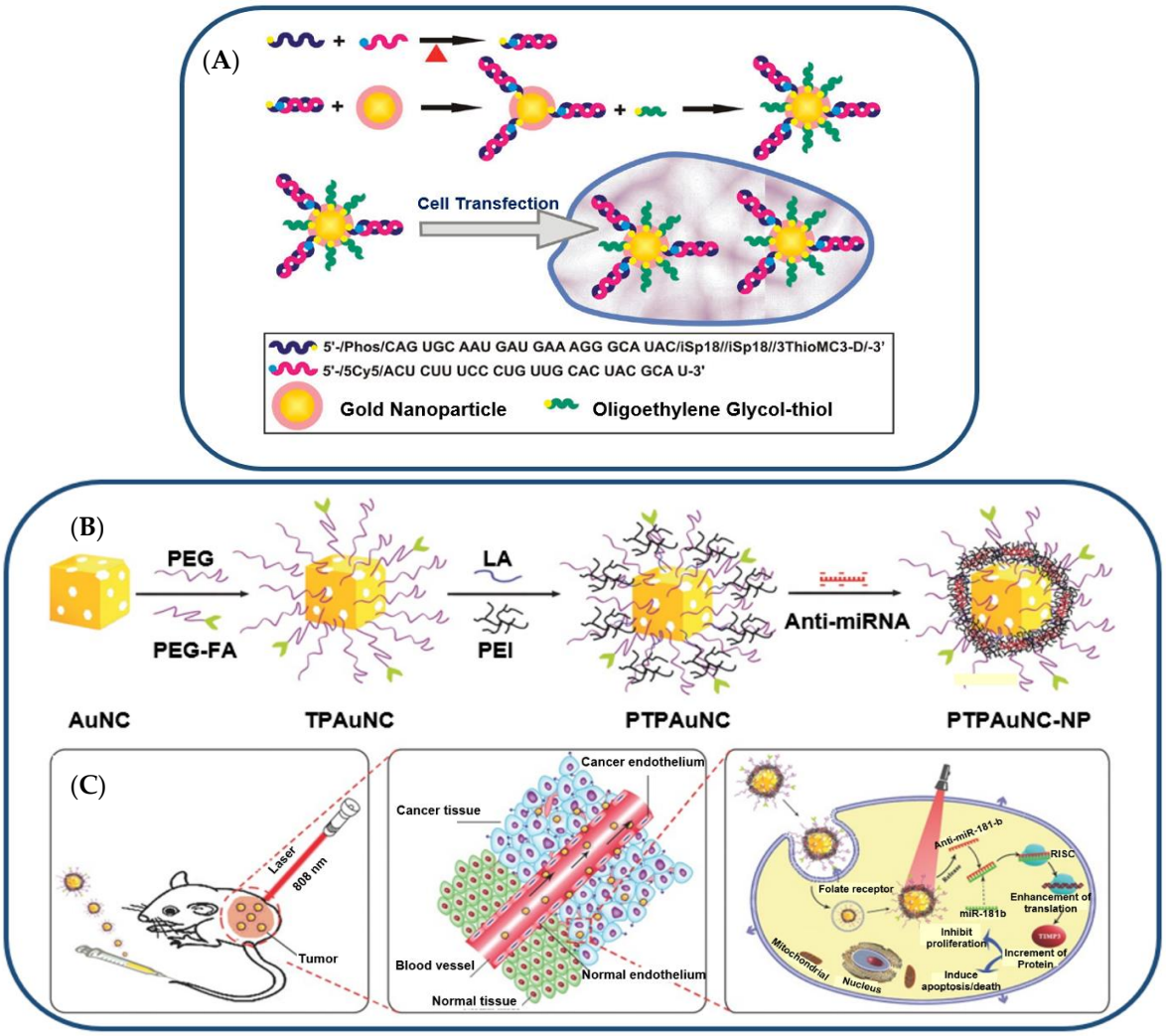

Figure 6. (**A**) Illustration (Not to Scale) of the Preparation of miRNA−AuNP Conjugates for Delivering miRNAs to Cells. Reproduced with permission from reference [113]. Copyright 2012 American Chemical Society. (**B**) Gold-nanocage-based targeted nanocomplex formulation process and (**C**) NIR-laser-induced targeted gene-photothermal therapy using the nanocomplexes. Adapted with permission from reference [118]. Copyright 2016 Wiley.

For functionalized miRNA delivery systems, there are few studies on the effect of nanoparticle size on cellular uptake, biodistribution, and tumor therapeutic efficacy [117]. Bao et al. designed miR-26a-loaded nanocomplexes (PPHAuNCs-TNCs) and investigated their cellular uptake, biodistribution, and therapeutic efficacy [117]. For miRNA delivery, 30 nm, 50 nm, and 70 nm PPHAuNCs-TNCs were developed [117]. All three systems condense miRNAs and inhibit their degradation by enzymes. Interestingly, PPHAuNCs-30-TNCs and PPHAuNCs-50-TNCs had greater tumor accumulation and cellular uptake than PPHAuNCs-70-TNC [117]. Compared to PPHAuNCs-50-TNCs, PPHAuNCs-30-TNCs demonstrated rapid and centralized tumor accumulation in xenograft and orthotopic HCC models [117].

In a separate study, researchers developed a nanocarrier-mediated RNA delivery system to deliver the tumor-suppressing miRNA-34a for triple-negative breast cancer TNBC [116]. miR-34a is ineffective as a therapeutic agent because nucleases degrade it, and it cannot passively enter cells. Consequently, nanocarriers are designed to boost miR-34a's stability and cellular entry [116]. As a plasmonic nanocarrier, a photo-responsive gold nanoshell (NS) with a silica core and a gold shell was created to release miRNA-34a in

response to continuous wave (CW) or nanosecond pulsed NIR light (Figure 7) [116]. The nanoshells were synthesized using a two-step process. First, small gold colloids were prepared using the Duff method [122], and these seed nanoparticles were used to decorate larger silica spheres. Next, the composite nanoparticles were mixed with $HAuCl_4$, potassium chloride, and formaldehyde to enable the formation of the gold shells. Synthesized NS was then coated with thiol-containing miR-34a or scrambled miR-co duplexes (Figure 7A,B). Electron microscopy confirmed 150 nm monodisperse miR-co/NS and miR-34a/NS conjugates (Figure 7C) [116]. In UV-visible spectroscopy, the peak extinction of NS after functionalization shifted toward the red (Figure 7D) [116]. MiRNA and PEG neutralized zeta potential and increased hydrodynamic diameter by 20 nm (Figure 7E) [116]. Using the OliGreen assay, miR-co/NS and miR-34a/NS had 7300 and 5500 duplexes, respectively (Figure 7F) [116]. This plasmonic NS-mediated delivery system efficiently delivered light-activated miRNA-34a to TNBC cells [116].

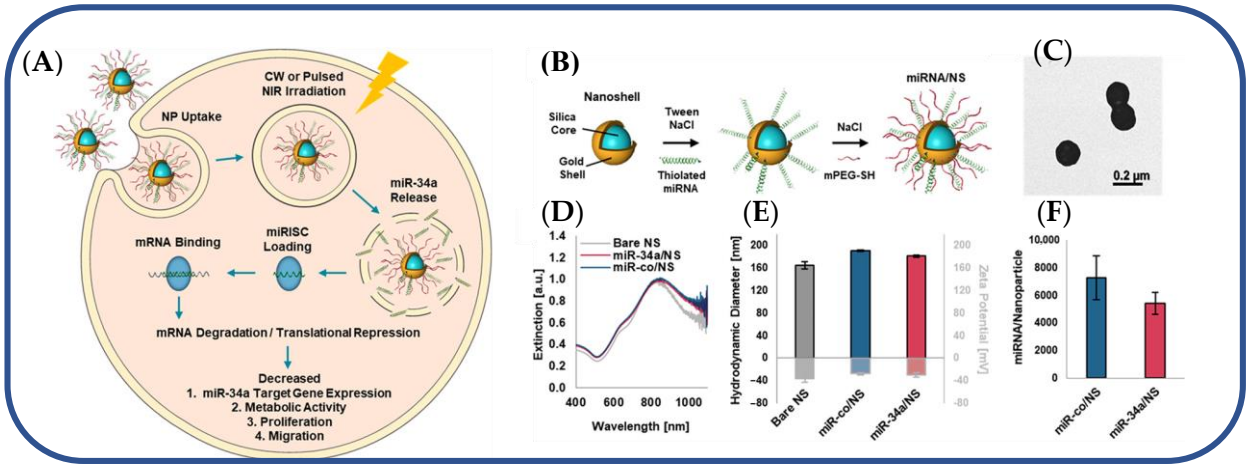

Figure 7. (**A**) Light-triggered release of miR-34a from nanoshells in TNBC cells. (**B**) Scheme depicting the process to coat NS with miRNA and Mpegsh. (**C**) Transmission electron micrograph of miR-co/NS. (**D**) Plasmon resonant extinction spectra comparing miRNA/NS conjugates to bare NS with peak extinction at 810 nm. (**E**) Hydrodynamic diameters (black outline) and zeta potential measurements (gray outline) of miRNA/NS conjugates and bare NS. (**F**) OliGreen analysis of miRNA loading on both miR34a/NS and miRco/NS. Reproduced with permission from reference [116]. Copyright 2021 American Chemical Society.

Ren et al. developed a sequential co-delivery system that increases anticancer efficacy by eightfold and anticancer stem cell activity by fiftyfold [115]. This system utilizes a stable, biocompatible, and near-infrared-radiation (NIR) responsive hollow gold nanoparticles (HGNPs) to co-deliver miR-21i/Dox, termed as D-P-HGNPs/21i [115]. Compared to solid gold nanoparticles, the hollow interior of HGNPs increased the drug payload [115]. As shown in Figure 8, HGNPs were modified with thiolated PAMAM dendrimers via a strong Au–S bond (Step I) [115]. The positively charged Dox was subsequently absorbed by HGNPs (Step II) [115]. On HGNPs, electrostatic interactions condensed miR-21i to PAMAM (Step III). TEM images and particle sizes of each step are shown in Figure 8B,C, respectively [115]. The D-P-HGNPs/21 entered the cells through the endocytic pathway [115]. Due to the proton sponge mechanism of the PAMAM dendrimer, miR-21i escaped the endosome and was released into the cytoplasm (Step V) after entering tumor cells (Step IV) [115]. This made cancer cells and cancer stem cells (CSCs) more sensitive to chemotherapy (Step VI) [115]. In four hours, NIR caused HGNPs to collapse (Step VIII) and caused the release of Dox (Step VIII) [115]. The sequential miR21i/Dox system eradicated cancer cells and cancer stem cells (CSCs) *in vitro* and *in vivo* and exhibited superior anti-cancer efficacy [115].

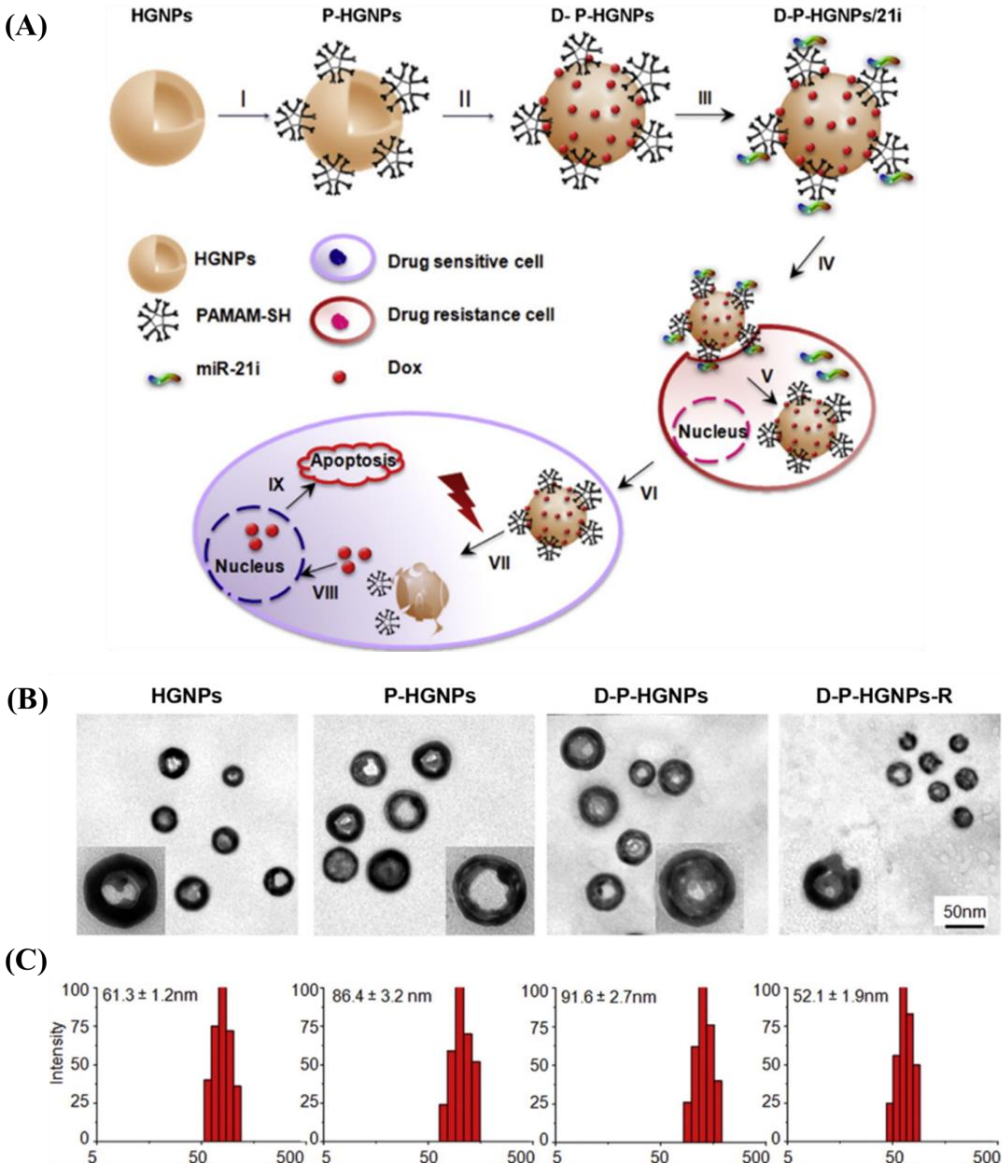

Figure 8. (**A**) Schematic illustration of gold-nanoparticle-based NIR triggered sequential miR-21 inhibitor/Dox release with precise time interval for optimal combination therapy. (I–III) Formation of HGNP-based co-delivery system. D-P-HGNPs/21i entered cells through endocytosis (IV). Upon entering the tumor cells, miR-21i was released first (V), modulating the intrinsic state to a more chemosensitive state (VI). At the desired time, application of NIR laser triggered collapse of HGNPs and a burst release of doxorubicin (VII), activating two apoptosis signaling pathways, thereby inducing the synergistic apoptosis response (IX). (**B**) TEM images of HGNPs, D-P-HGNPs, D-P-HGNPs, and D-P-HGNPs-R. (**C**) Particle size measured by DLS. Adapted with permission from reference [115]. Copyright 2016 Elsevier.

Sukumar et al. investigated intranasal delivery of molecularly targeted theranostic nanoformulations against glioblastoma (GBM) in a recent study [120].

Figure 9 depicts the development of polyfunctional gold-iron oxide nanostar particles (polyGIONs) for the delivery of antimiR-21 and miR-100, which selectively target and combat GBM and enhance TMZ chemotherapy [120]. PolyGIONs are surface-functionalized with chitosan-cyclodextrin (CD-CS) hybrid polymers [120]. CD-CS coating increased the NPs' surface potential from +15 mV to +39 mV due to the positively charged free amine groups of chitosan [120]. This functionalization offers an efficient platform for surface loading negatively charged miRNAs via electrostatic interaction, while restricting

nanoparticle size to less than 50 nm for efficient intranasal delivery [120]. This therapeutic nanocarrier system was designed to treat GBM through nasal administration, bypassing the blood–brain barrier [120].

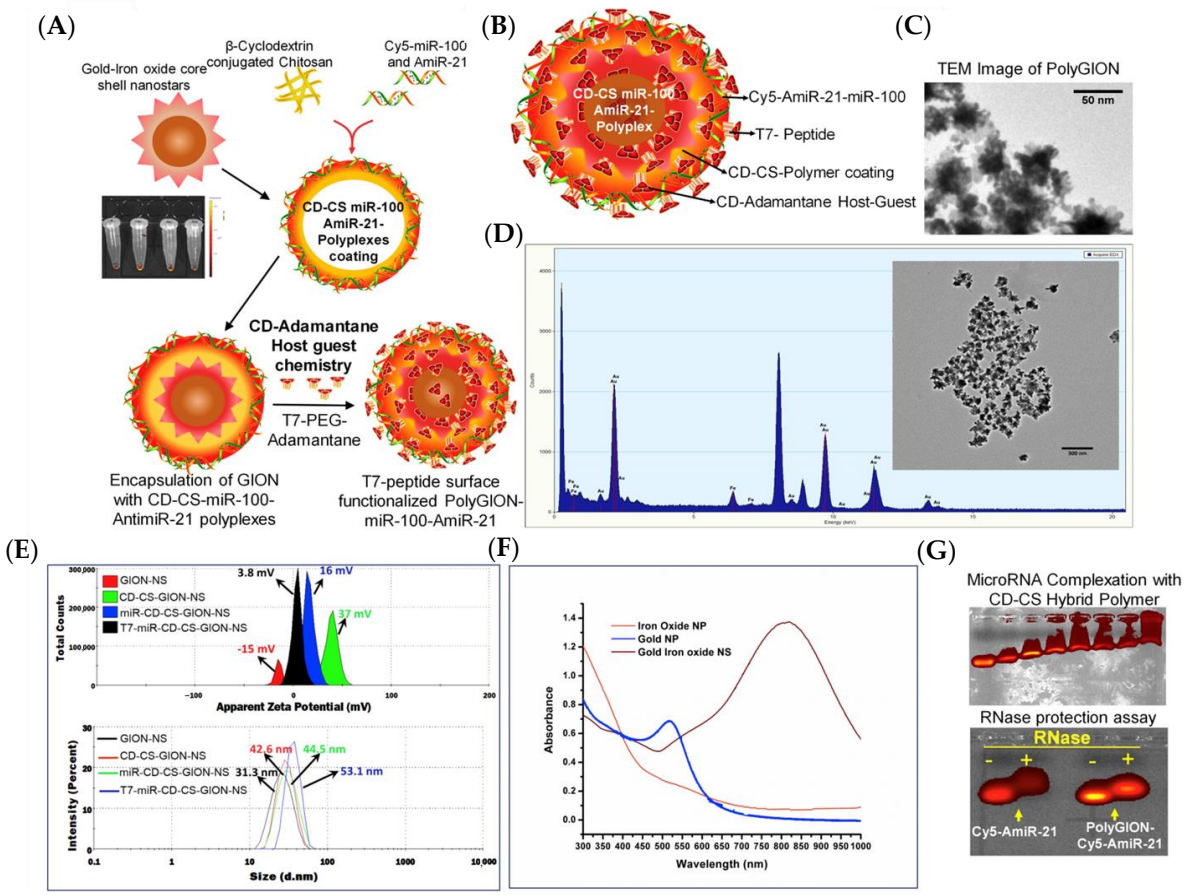

Figure 9. (**A**) Schematic illustration of synthesis of PolyGIONs and fluorescence images of Cy5-labeled miR-100 and antimiR-21-loaded CD-CS complexes. (**B**) Schematic representation of as-prepared polyGION structure and their various compositions. (**C**) TEM micrograph of GION. (**D**) GION coated with miR-100/antimiR-21 encapsulated CD-CS polymer layer, its EDS analysis, and corresponding images. (**E**) DLS measuring zeta potential and size of nanoparticles after each step of GION surface modification. (**F**) UV-vis spectra of as-prepared GION NS and its precursor nanoparticles. (**G**) Gel retardation assay for Cy5-miR-100/antimiR-21 encapsulation in CD-CS hybrid polymer and RNase protection assay for measuring the stability of encapsulated miRNAs in polyGION-CD-CS. Adapted with permission from reference [120]. Copyright 2019 Elsevier.

7. Nanoparticles for miRNA Diagnostics

Cancer has been identified as one of the most serious diseases with a high death rate [123]. Meanwhile, it is possible to decrease the death rate by early diagnosis of cancer [123] when the development of the cancerous cells causes the abnormal expression of miRNA [124]. Moreover, miRNAs can regulate gene expression at the post-transcriptional level, and they have been recognized as ideal biomarker candidates for early cancer diagnosis [123]. Conventional methods for the identification of miRNA, such as Northern blotting, microarray, and polymerase chain reaction (PCR), usually have low sensitivity and selectivity due to the intrinsic characteristics of miRNAs such as short length, high degradability, and low cellular abundance [125]. To resolve the inadequacy of sensitivity and selectivity, researchers have been using various amplifying strategies such as nanoparticle enhancement and isothermal amplification methods including nuclease-assisted reactions (i.e., target recycling processes induced by various nucleases such as duplex-specific nuclease

(DSN)) and enzyme-free reactions (i.e., independent from the enzyme, such as toehold-mediated strand displacement (TMSD)) [123,125]. In this section, we discuss different types of biosensors utilizing plasmonic nanoparticles for the quantitative analysis of miRNAs such as colorimetric, fluorescent, surface plasmon resonance (SPR), surface-enhanced Raman scattering (SERS), chemiluminescence biosensor, electrochemical biosensors, etc. [123]. Selected nanoparticle systems used for miRNA diagnostics are summarized in Table 2.

Yu et al. reported a cascade amplification strategy by combining DSN-assisted target recycling and TMSD-based catalytic hairpin assembly (CHA) reaction to develop an electrochemical biosensor for miRNA with high sensitivity and selectivity (Figure 10) [125]. In this biosensor, a hairpin probe (HP) HP1 was hybridized and unfolded in the presence of target miRNA that can form DNA/RNA heteroduplexes and activate DSN which was inactive before [124,125]. Then, DSN cleaved the DNA and released RNA and connector DNA in a process named DSN-assisted target recycling [125]. Next, connector DNAs opened the hairpin HP2, which was immobilized on the Au electrode, and hybridized to it via the TMSD reaction [125]. On the other hand, thiolated hairpins HP2 and HP3 were immobilized on the AuNPs, and they were introduced to the connector DNA-HP2 intermediate in order to make the interaction between HP3 and the exposed region of HP2 through a secondary TMSD reaction [125]. Consequently, these CHA reactions led to a self-assembly of AuNP hotspots on the Au electrode [125].

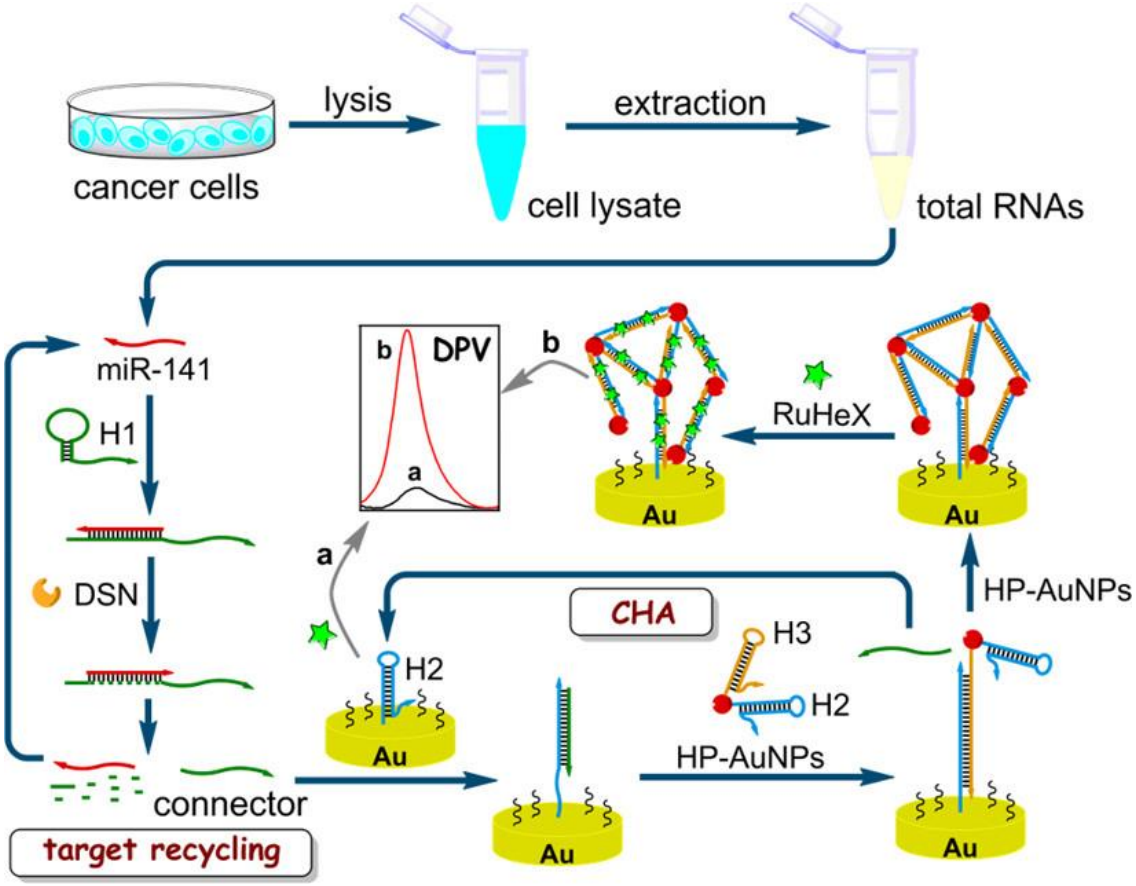

Figure 10. Electrochemical biosensor constructed from DSN-assisted target recycling and TMSD-based catalytic hairpin assembly (CHA) where an amplified "b" and a weak "a" electrochemical signals are measured by differential pulse voltammetry (DPV) in the presence of miR-141 and in the absence of miR-141, repectively. Reprinted (adapted) with permission from [125]. Copyright 2018 American Chemical Society.

Table 2. Nanoparticles for miRNA Diagnostics.

Plasmonic Substrate	Morphology	Type of Biosensor	Size (nm)	Conjugate	Target miRNA	Target Cell	Ref.
Au	Nanosphere (AuNPs)	Electrochemical	13	Thiol-labeled hairpin DNA	miR-141	Breast cancer	[125]
		Colorimetric	19	Thiolated probe	miRNA-155	Cancer cells	[126]
		Colorimetric	22	Thiolated RNA probes	miRNA-148a	Gastric cancer	[127]
		Colorimetric	20–30	Thiol-modified DNA	miR-21 and miR-155	Cancer cells	[128]
		Colorimetric and FRET	13	Thiol-modified hairpin probe	miRNA-21	Cancer cells	[124]
		FRET	13	Thiol-modified oligonu-cleotides	miR-21 and miR-141	Cancer cells	[129]
		Thermophoretic	13	Thiol-modified single-stranded DNA	miR-375	Breast cancer	[130]
		Dark-field	50	Thiolated DNA	miRNA	-	[131]
	Nanospike	PRAM	100	Thiolated DNA	miR-375	Prostate cancer	[132]
	Nanorod (AuNRs)	PEF	27 × 12	Thiolated DNA	miRNA-21	Cancer cells	[133]
		FRET	60	Thiolated DNA	miR-21 and miR-200b	Cancer cells	[134]
	Nanocubes (AuNCs)	SPR	50	Thiol-modified single-strand DNA	miRNA-205	Lung cancer	[135]
	Nanostripes	SPR	200 × 100	Thiolated DNA	miRNA-125b	-	[136]
	Mountaintop-shaped nanopillar	SERS	800 × 200	Thiol-modified DNA	miRNA-10b, miRNA-21, and miRNA-373	Cancer Cells	[137]
Ag	Nanosphere (AgNPs)	SERS	110	Thiolated DNA	miRNA-21	Cancer cells	[87]
	Nanoparticle films (AgNFs)	SERS	-	MBA-ssDNA, DSNB-ssDNA, and 6TG-ssDNA	miR-26a-5p, miR-223, and miR-27a-3p	Liver cancer	[138]
Au-Ag	Nanosphere	SPR	13	Thiolated DNA	miRNA-21	Cancer cells	[123]
Au@MoS_2	Nanosphere	SPR	10	Thiol-modified DNA	miRNA-141	Cancer cells	[139]
Au@graph-ene oxide	Nanosphere (AuNPs-GO)	SPR	18	Thiolated capture DNA probe	miRNA-141	Prostate cells	[140]
Fe_3O_4@Au	Nanospike	PRAM	90	SH-PEG-SA-B-DNA	miR-375	Prostate cancer	[141]
Au@Pt	Nanosphere	FRET	16	Thiol-modified single-stranded DNA	miRNA-21	Cancer cells	[89]
Au@Fe_2O_3	Nanocube	Electrochemical	-	MB-SA-B-DNA	miR-107	Cancer cells	[142]
Pd	Nanosphere (PdNPs)	Electrochemical	30	Thiolated miRNA-155 primer	miRNA-155	Oncogenesis	[88]
Au-Ni-Au	Nanorod	MEF	267 × 745	Thiolated molecular beacon and anti-CD63	miRNA-124	Stem cell neurogenesis	[143]

Magnetic nanoparticles have also been used in biosensors. Islam et al. developed an electrochemical biosensor using gold-loaded cubic nanoporous ferric oxide on a screen-printed carbon electrode (SPCE) (Figure 11A) [142]. Paramagnetic cubic nanoparticles

are suitable for magnetic purification, with high electrocatalytic activity toward RuHex and a large gold surface area to adsorb target miRNA [142]. Islam et al. synthesized biotinylated-capture probes attached to streptavidin-functionalized magnetic beads (MB-SA) by a biotin–avidin interaction (MB-SA-B-DNA) [142]. Target miRNA were hybridized to the capture probe and isolated magnetically [142]. Then, purified miRNA was released from the magnetic beads by heat and adsorbed directly on the Au-loaded nanoporous iron oxide nanocubes via RNA–gold interactions [142]. Finally, nanocubes with target miRNA were immobilized magnetically on the SPCE, and the electrochemical signal was further amplified by $[Fe(CN)_6]^{3-}$ [142]. In another study, Che et al. reported photonic resonator absorption microscopy (PRAM) as an imaging-based biosensor in which AuNPs with a magnetic core could be visualized on a photonic crystal (PC) surface (Figure 11B) [141]. Che et al. synthesized magneto-plasmonic nanoparticles (MPNPs) by developing Fe_3O_4@Au core-shell nanoparticles. The MPNPs were coated with SH-PEG-NHS and conjugated to streptavidin (SA) [141]. Next, biotin-DNA (B-DNA) was annealed to a protector and immobilized on the MPNPs via biotin–avidin interactions to give SH-PEG-SA-B-DNA. In this imaging-based detection method, the protector strand can be removed in the presence of target miRNA, and probe-MPNPs can be activated through TMSD [141]. Then, the activated MPNPs were captured by the DNA probes on the PC surface [141]. An external magnetic field placed below the PC concentrated the magneto-plasmonic nanoparticles near the PC surface and decreased the response time, which was limited by mass transfer in a previous study [132].

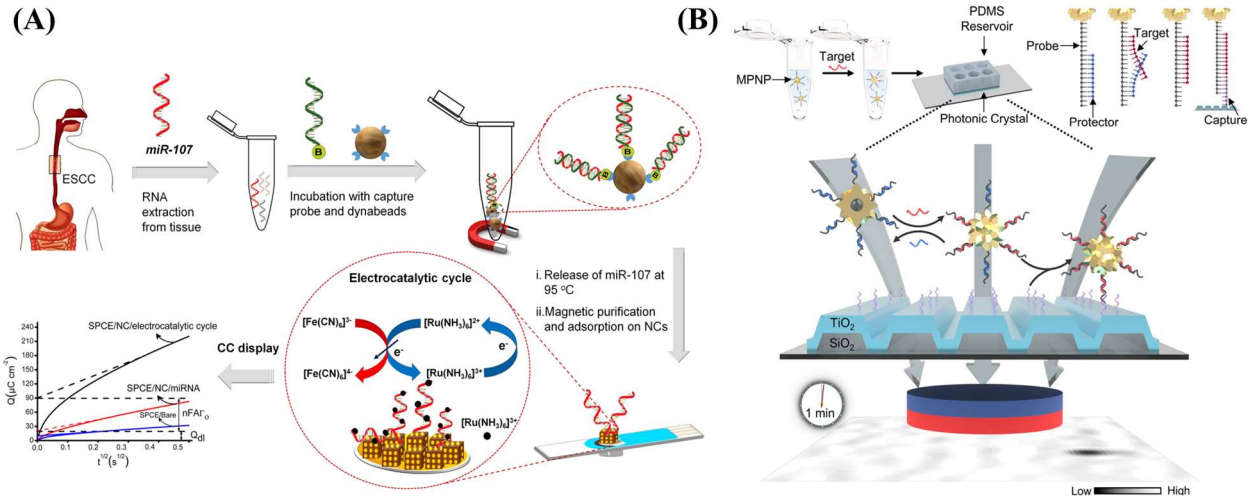

Figure 11. (**A**) Purification of miRNA-107 by streptavidin-functionalized (blue part) magnetic beads (Dynabeads) followed by electrochemical measurements of the miRNA-deposited gold-loaded cubic nanoporous ferric oxide on the SPCE (light blue surface). Reprinted from [142], Copyright 2018, with permission from Elsevier. (**B**) Photonic resonator absorption microscopy (PRAM) utilizing magneto-plasmonic nanoparticles (MPNPs) on the photonic crystal (PC) surface constructed from (TiO_2-SiO_2). Reprinted (adapted) with permission from [141]. Copyright 2022 American Chemical Society.

Diseases are usually associated with more than one biomarker [125], and fluorescence imaging analysis makes it possible to detect two sets of immobilized fluorophore-labeled DNAs on AuNPs to simultaneously detect two distinct target miRNA inside live cells [129]. Moreover, this is useful since some diseases could change the expression of multiple miRNAs [129]. Huang et al. developed a dual-mode sensor constructed from a colorimetric and fluorescent mode sensor to detect miRNA based on the DSN-assisted signal amplification technique [124]. Enzyme-assisted methods have high sensitivity, but they suffer from costly experimental procedure, limited selectivity, and design complexity that limit the practical applications of this method, so these drawbacks have led to the use of DSN [124]. In this work, Huang et al. immobilized dye-labeled thiolated-hairpin probes on the AuNPs,

by forming S-Au bonds, in order to release fluorophores in each round of DSN-assisted target recycling [124]. On the other hand, many DNA-modified AuNPs were formed after each hybridization in which the electrostatic repulsion between them could be diminished, causing aggregation that can be observed as a color change from red to blue [124]. It should be considered that intracellular biothiols can cleave the Au-S bond and increase the background signals in cell imaging [89]. However, the Pt-S bond is more stable than Au-S, and coating AuNPs with a thin layer of platinum can improve the stability of thiolated DNA on AuNPs@Pt while optical properties were retained [89].

Gold nanorods (AuNRs) are another type of nanoparticles, and researchers can take advantage of their morphology and develop a controllable modification of thiolated-ssDNA on the sides or ends [134]. Qu et al. developed a core-satellite biosensor with zeptomolar sensitivity in which AuNRs are surrounded by upconverting nanoparticles (UCNPs) such as $NaGdF_4$ [134]. For this purpose, Qu et al. utilized AuNRs to modify the ends and sides of rods with thiolated DNA_2 and thiolated DNA_5, respectively [134]. Furthermore, dye-modified DNA_3 and DNA_5 were linked to the UCNPs by DNA_1 and DNA_4, respectively. Finally, core-satellite geometry was formed by the hybridization of DNA1 to DNA2 and DNA4 to DNA5 [134]. In the presence of target miRNA, UCNPs disassembled from AuNRs by hybridization followed by transferring energy between UCNPs and dye molecules that led to the lighting up of dye [134]. Hence, biosensors can simultaneously quantify two miRNAs (i.e., miRNA-21 and miRNA-200b) by detecting the excitation of dyes [134]. In another research, Peng et al. used AuNRs to generate a strong electromagnetic field in a form of nanogap antennas (Figure 12) [133]. AuNRs can be used in the plasmon-enhanced fluorescence (PEF) technique in which AuNRs would act as a nanoantenna to enhance the fluorescence signals through coupling between the emitter and the LSPR of AuNRs [133]. Peng et al. immobilized two different DNA hairpins (i.e., thiolated dye-modified hairpin H1 and thiolated hairpin H2) on the ends of PEG-decorated AuNRs [133]. In the presence of target miRNA, H1 would be opened by hybridization and get exposed to H2 resulting in a H1-H2 duplex in which the dye would be placed in between end-to-end coupled AuNRs and would enhance the fluorescence signal [133]. Based on the distance between the dye and AuNRs, the dye could get quenched by AuNRs due to fluorescence resonance energy transfer (FRET) [133].

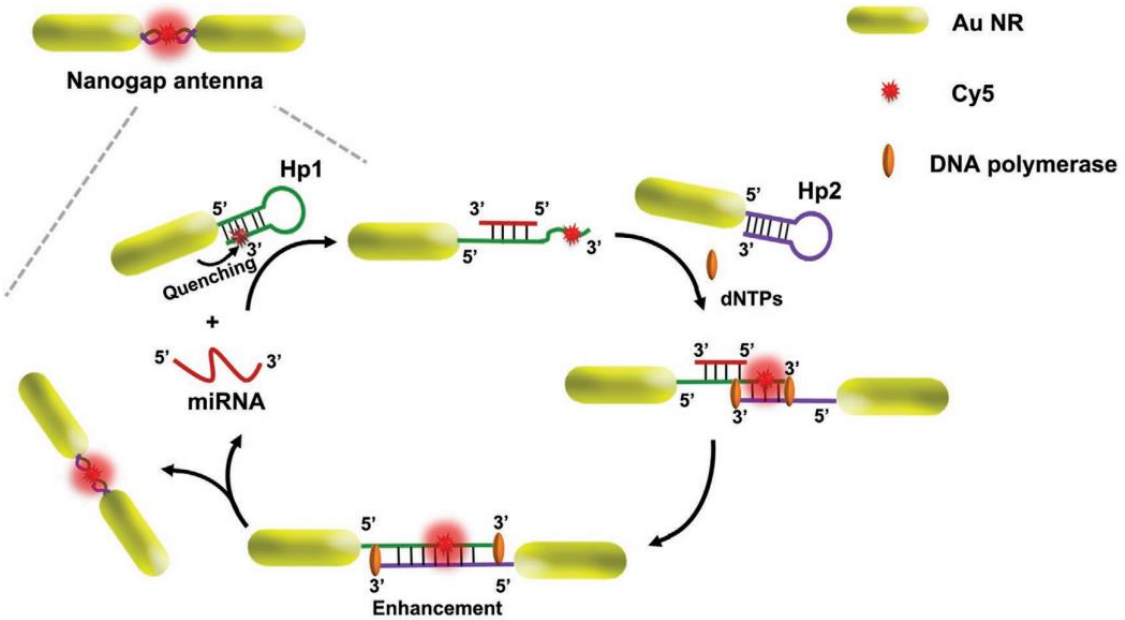

Figure 12. Assembly of AuNRs to create nanogap antennas.Reprinted with permission from Ref. [133]. Copyright 2020, Wiley-VCH GmbH.

There are other strategies to increase the concentration of released nanoflares such as using a thermophoretic sensor [130]. Thermophoresis is a phenomenon in which particles migrate along a temperature gradient [130]. A thermophoretic sensor could be utilized to detect target miRNA without the need of extracting miRNA or the amplification of the target miRNA [130]. Zhao et al. developed a thermophoretic sensor to detect breast cancer at early stages (stage I and II). In this sensor, thiolated-recognition DNA and its complementary nanoflare-modified DNA were immobilized on the AuNPs [130]. Target miRNA would hybridize probe DNA and release nanoflares which could be thermophoretically accumulated by localized laser heating to enhance the intensity of fluorescence [130].

Liu et al. developed an enzyme-free SPR biosensor by immobilizing a hairpin probe on the Au film (SAMs) to capture DNA miRNA with high sensitivity and selectivity (Figure 13A) [123]. First, miRNA was isolated and purified by using MB-SA-B-DNA, as it was described previously [142]. Next, Au surface was passivated by 6-mercapto-1-hexanol (MCH) to decrease the non-specific binding of DNA and make DNA stand on the Au surface as a self-assembled monolayer with the van der Waals interaction between MCH and DNA [123]. In the presence of target miRNA, the stem-loop structure of the DNA, on the Au surface, was unfolded, and DNA on the AuNPs can be bound to the Au surface by hybridization and forming a DNA super sandwich. Therefore, an enhancement of the shift in the resonance angle would be resulted from the electronic coupling between nanoparticles' localized plasmon and Au film's surface plasmon [123]. Then, positively charged AgNPs were attached to the negatively charged DNA super sandwich and further improved the shift in the resonance angle [123]. However, the whole procedure is time consuming and complicated, and further research is required to reduce the assay time and enhance the convenience of the procedure [123]. Zhang et al. used gold nanocubes instead of gold nanospheres because of their nanocrystal configuration in which more vertexes in nanocubes enhance SPR in a broader energy range compared to the nanospheres [135]. In this study, Zhang et al. developed an SPR nanoprobe to detect trace lung cancer marker miRNA with a limit of detection of 5 pM that is three orders of magnitude more sensitive than nanosphere's [135]. For this purpose, Zhang et al. immobilized thiolated single-strand DNA (ssDNA) on AuNCs to monitor LSPR peak shift that can be resulted from the hybridization between AuNCs-ssDNA and target miRNA [135]. Performance of the SPR biosensor can be enhanced by using molybdenum sulfide (MoS_2) (Figure 13B) [139]. Nie et al. used MoS_2 as a reducing agent to synthesize AuNPs where the edge or defective sites of a MoS_2 nanosheet can be decorated by AuNPs [139]. In this sensor, a thiolated probe and DNA were immobilized on a Au film and AuNPs, respectively [139]. Target miRNA can construct a sandwich structure including Au film and AuNPs-MoS_2 nanocomposites that increased the SPR signal [139]. In another research, Wang et al. used graphene oxide-AuNPs hybrids to provide a large surface area for loading numerous AuNPs near the Au film in order to enhance the SPR signal [140].

Thiol-functionalized miRNA can be characterized by surface-enhanced Raman scattering (SERS) to detect miRNAs and dye on AuNPs and gel electrophoresis to analyze the binding and stability of miRNA on AuNPs [113]. Chen et al. developed an enzyme-free SERS biosensor using mismatched CHA reactions (Figure 14) [87]. SERS signals were obtained from the aggregation of nanoparticles in the liquid phase resulting unreliable SERS signals while Chen et al. deposited AgNPs on a silicon wafer to prevent aggregation of nanoparticles and reached reproducible and reliable signals [87]. Moreover, 4-aminothiophenol (4-ATP) was used to serve as an internal standard to calibrate signal fluctuation [87]. In this study, thiolated DNA was immobilized on AgNPs-Si; the AgNPs were previously coated with 4-ATP [87]. In the presence of target miRNA, dye-labeled hairpin H1 was hybridized with it, and it was unfolded and exposed to a mismatched H2 which initiated the hybridization of H1 with H2 via a CHA reaction and released the target miRNA to repeat the same procedure many times [87]. Finally, dye-labeled H1-H2 duplexes were captured by DNA on the SERS substrate and generated an enhancement in the SERS signal assisted by the SPR of AgNPs-Si [87]. Scattering peaks can also be measured

with a dark-field microscope, but it is an expensive and complex instrument [131]. Hwu et al. developed a miniaturized dark-field setup, named dark-field microwells, to detect scattering-based nanoparticles [131]. The developed setup is not time consuming, and it can be fabricated on silicon wafers and produced at the industrial scale at a low cost [131].

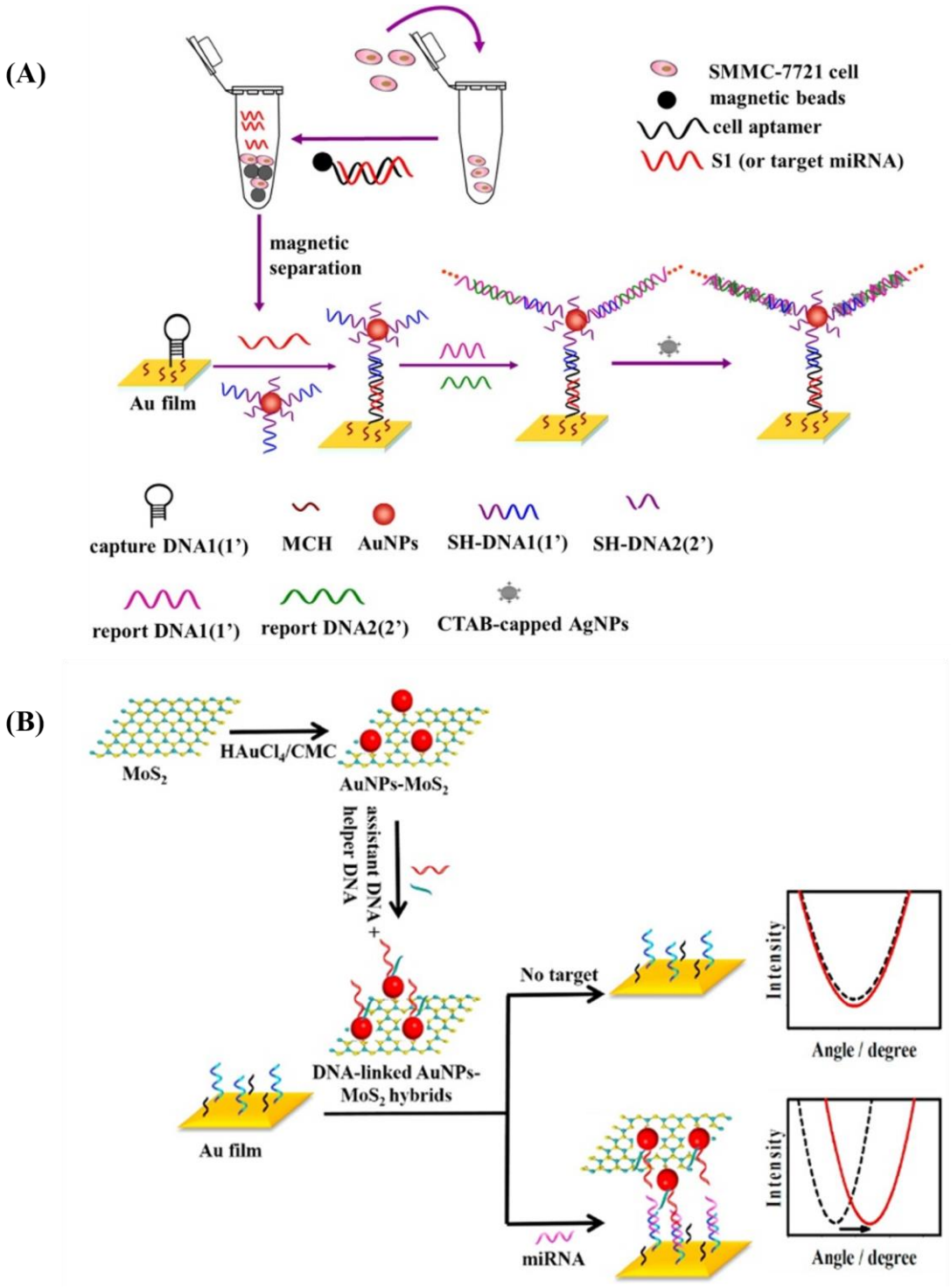

Figure 13. (**A**) Purification of target miRNA followed by hybridization to the Au film with immobilized DNA in an enzyme-free SPR biosensor. Reprinted from [123], Copyright 2017, with permission from Elsevier. (**B**) SPR biosensor constructed from AuNPs-MoS_2 nanocomposites to enhance SPR signal. Reprinted from [139], Copyright 2017, with permission from Elsevier.

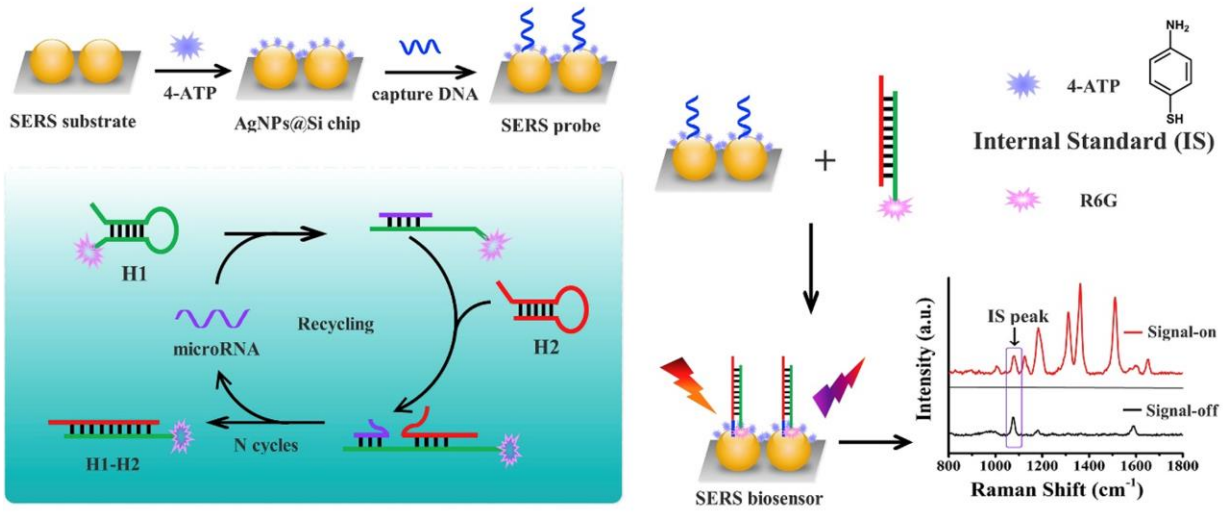

Figure 14. AgNPs in an enzyme-free SERS biosensor using mismatched CHA reactions. Reprinted from [87], Copyright 2019, with permission from Elsevier.

8. Conclusions

The use of miRNA is a highly effective therapeutic alternative to chemotherapy but is hindered by degradation during passive circulation. Attaching miRNA onto a nanocarrier has evolved as a new method of delivery. However, cellular uptake is still dependent on the nanoparticle shape, size, and charge. Based on the route taken to develop the nanoparticle, the surfactant used can have an effect on particle uptake. Furthermore, the use of adsorbates can offer a binding platform for oligonucleotides onto inorganic particles through covalent and noncovalent bonds. The binding of the oligonucleotides onto the surface can provide substantial carrier capability to deliver miRNA into cells. Regardless, the degradation of the oligonucleotides is another challenge that needs further focus and research.

Author Contributions: J.H., P.T., M.O., M.D.M., O.K., W.T., C.-H.L., A.K., H.-V.T., P.H.G. and T.R.L. discussed, commented on, and wrote the manuscript. All authors have read and agreed to the published version of the manuscript.

Funding: We thank the National Science Foundation (CHE-2109174) and the Robert A. Welch Foundation (Grant No. E-1320) for generously supporting this research.

Institutional Review Board Statement: Not applicable.

Informed Consent Statement: Not applicable.

Data Availability Statement: Not applicable.

Conflicts of Interest: The authors declare no competing financial interests.

References

1. Guyon, N.; Garnier, D.; Briand, J.; Nadaradjane, A.; Bougras-Cartron, G.; Raimbourg, J.; Campone, M.; Heymann, D.; Vallette, F.M.; Frenel, J.-S.; et al. Anti-PD1 Therapy Induces Lymphocyte-Derived Exosomal MiRNA-4315 Release Inhibiting Bim-Mediated Apoptosis of Tumor Cells. *Cell Death Dis.* **2020**, *11*, 1048. [CrossRef]
2. He, Z.; Li, W.; Zheng, T.; Liu, D.; Zhao, S. Human Umbilical Cord Mesenchymal Stem Cells-Derived Exosomes Deliver MicroRNA-375 to Downregulate ENAH and thus Retard Esophageal Squamous Cell Carcinoma Progression. *J. Exp. Clin. Cancer Res.* **2020**, *39*, 140. [CrossRef]
3. Masoumi-Dehghi, S.; Babashah, S.; Sadeghizadeh, M. MicroRNA-141-3p-Containing Small Extracellular Vesicles Derived from Epithelial Ovarian Cancer Cells Promote Endothelial Cell Angiogenesis through Activating the JAK/STAT3 and NF-KB Signaling Pathways. *J. Cell Commun. Signal.* **2020**, *14*, 233–244. [CrossRef]
4. Zhang, M.; Shi, Y.; Zhang, Y.; Wang, Y.; Alotaibi, F.; Qiu, L.; Wang, H.; Peng, S.; Liu, Y.; Li, Q.; et al. MiRNA-5119 Regulates Immune Checkpoints in Dendritic Cells to Enhance Breast Cancer Immunotherapy. *Cancer Immunol. Immunother.* **2020**, *69*, 951–967. [CrossRef]

5. Hodge, J.; Wang, F.; Wang, J.; Liu, Q.; Saaoud, F.; Wang, Y.; Singh, U.P.; Chen, H.; Luo, M.; Ai, W.; et al. Overexpression of MicroRNA-155 Enhances the Efficacy of Dendritic Cell Vaccine against Breast Cancer. *OncoImmunology* **2020**, *9*, 1724761. [CrossRef]
6. Zhao, H.; Li, T.; Yao, C.; Gu, Z.; Liu, C.; Li, J.; Yang, D. Dual Roles of Metal–Organic Frameworks as Nanocarriers for MiRNA Delivery and Adjuvants for Chemodynamic Therapy. *ACS Appl. Mater. Interfaces* **2021**, *13*, 6034–6042. [CrossRef]
7. De Haan, P.; Van Diemen, F.R.; Toscano, M.G. Viral Gene Delivery Vectors: The next Generation Medicines for Immune-Related Diseases. *Hum. Vaccines Immunother.* **2021**, *17*, 14–21. [CrossRef]
8. Wang, J.; Yu, L.; Zhou, A.; Liu, J.; Wang, K.; Luo, Y.; Wang, F. Non-Viral Gene Delivery Systems for Treatment of Myocardial Infarction: Targeting Strategies and Cardiac Cell Modulation. *Pharmaceutics* **2021**, *13*, 1520. [CrossRef]
9. Tasset, A.; Bellamkonda, A.; Wang, W.; Pyatnitskiy, I.; Ward, D.; Peppas, N.; Wang, H. Overcoming Barriers in Non-Viral Gene Delivery for Neurological Applications. *Nanoscale* **2022**, *14*, 3698–3719. [CrossRef]
10. Rodriguez, D.; Marquez, M.D.; Zenasni, O.; Han, L.T.; Baldelli, S.; Lee, T.R. Surface Dipoles Induce Uniform Orientation in Contacting Polar Liquids. *Chem. Mater.* **2020**, *32*, 7832–7841. [CrossRef]
11. Bhardwaj, A.; Pandey, L.M. Design of Antibiofilm Surfaces by Immobilization of Biogenic Silver Nanoparticles on Amine Self-Assembled Monolayers. *Mater. Lett.* **2022**, *311*, 131574. [CrossRef]
12. Durainatarajan, P.; Prabakaran, M.; Ramesh, S. Self-Assembled Monolayers of Novel Imidazole Derivative on Copper Surface for Anticorrosion Protection in Neutral Medium. *J. Adhes. Sci. Technol.* **2021**, *35*, 2580–2601. [CrossRef]
13. Pathak, P.; Cho, H.J. Self-Assembled 1-Octadecanethiol Membrane on Pd/ZnO for a Selective Room Temperature Flexible Hydrogen Sensor. *Micromachines* **2022**, *13*, 26. [CrossRef] [PubMed]
14. Singhana, B.; Jamison, A.C.; Hoang, J.; Lee, T.R. Self-Assembled Monolayer Films Derived from Tridentate Cyclohexyl Adsorbates with Alkyl Tailgroups of Increasing Chain Length. *Langmuir* **2013**, *29*, 14108–14116. [CrossRef] [PubMed]
15. St. Hill, L.R.; Craft, J.W.; Chinwangso, P.; Tran, H.-V.; Marquez, M.D.; Lee, T.R. Antifouling Coatings Generated from Unsymmetrical Partially Fluorinated Spiroalkanedithiols. *ACS Appl. Bio Mater.* **2021**, *4*, 1563–1572. [CrossRef]
16. St. Hill, L.R.; Tran, H.-V.; Chinwangso, P.; Lee, H.J.; Marquez, M.D.; Craft, J.W.; Lee, T.R. Antifouling Studies of Unsymmetrical Oligo(Ethylene Glycol) Spiroalkanedithiol Self-Assembled Monolayers. *Micro* **2021**, *1*, 151–163. [CrossRef]
17. Tajalli, P.; Hernandez Rivera, J.M.; Omidiyan, M.; Tran, H.-V.; Lee, T.R. Carbonate-Terminated Self-Assembled Monolayers for Mimicking Nanoscale Polycarbonate Surfaces. *ACS Appl. Nano Mater.* **2023**, *6*, 2472–2477. [CrossRef]
18. Wang, L.; Schubert, U.S.; Hoeppener, S. Surface Chemical Reactions on Self-Assembled Silane Based Monolayers. *Chem. Soc. Rev.* **2021**, *50*, 6507–6540. [CrossRef]
19. Auzelle, T.; Ullrich, F.; Hietzschold, S.; Sinito, C.; Brackmann, S.; Kowalsky, W.; Mankel, E.; Brandt, O.; Lovrincic, R.; Fernández-Garrido, S. External Control of GaN Band Bending Using Phosphonate Self-Assembled Monolayers. *ACS Appl. Mater. Interfaces* **2021**, *13*, 4626–4635. [CrossRef]
20. Jiang, C.; Huang, F.; Chen, Y.; Jiang, L. Highly Uniform Self-Assembled Monolayers of Silver Nanospheres for the Sensitive and Quantitative Detection of Glutathione by SERS. *Dalton Trans.* **2021**, *50*, 10436–10445. [CrossRef]
21. Sakunkaewkasem, S.; Gonzalez, M.A.; Marquez, M.D.; Lee, T.R. Olefin-Bridged Bidentate Adsorbates for Generating Self-Assembled Monolayers on Gold. *Langmuir* **2020**, *36*, 10699–10707. [CrossRef]
22. Hoang, J.; Park, C.S.; Marquez, M.D.; Gunaratne, P.H.; Lee, T.R. DNA Binding on Self-Assembled Monolayers Terminated with Mixtures of Ammonium and Trimethylammonium Groups: Toward a Gene-Delivery Platform. *ACS Appl. Nano Mater.* **2020**, *3*, 6621–6628. [CrossRef]
23. Yu, T.; Marquez, M.D.; Tran, H.-V.; Lee, T.R. Crosslinked Organosulfur-Based Self-Assembled Monolayers: Formation and Applications. *Soft Sci.* **2022**, *2*, 5. [CrossRef]
24. Sánchez-Paniagua, M.; Palenzuela-Batista, S.; Manzanares-Palenzuela, C.L.; López-Ruiz, B. Electrochemical Genosensor for Klotho Detection Based on Aliphatic and Aromatic Thiols Self-Assembled Monolayers. *Talanta* **2020**, *212*, 120735. [CrossRef] [PubMed]
25. Hoang, J.; Park, C.S.; Lee, H.J.; Marquez, M.D.; Zenasni, O.; Gunaratne, P.H.; Lee, T.R. Quaternary Ammonium-Terminated Films Formed from Mixed Bidentate Adsorbates Provide a High-Capacity Platform for Oligonucleotide Delivery. *ACS Appl. Mater. Interfaces* **2018**, *10*, 40890–40900. [CrossRef] [PubMed]
26. Diener, C.; Keller, A.; Meese, E. Emerging Concepts of MiRNA Therapeutics: From Cells to Clinic. *Trends Genet.* **2022**, *38*, 613–626. [CrossRef] [PubMed]
27. Friedman, R.C.; Farh, K.K.-H.; Burge, C.B.; Bartel, D.P. Most Mammalian MRNAs Are Conserved Targets of MicroRNAs. *Genome Res.* **2009**, *19*, 92–105. [CrossRef]
28. Liu, B.; Shyr, Y.; Cai, J.; Liu, Q. Interplay between MiRNAs and Host Genes and Their Role in Cancer. *Brief. Funct. Genom.* **2019**, *18*, 255–266. [CrossRef]
29. Roberts, T.C. The MicroRNA Biology of the Mammalian Nucleus. *Mol. Ther. Nucleic Acids* **2014**, *3*, e188. [CrossRef]
30. Kim, Y.-K.; Kim, V.N. Processing of Intronic MicroRNAs. *EMBO J.* **2007**, *26*, 775–783. [CrossRef]
31. He, C.; Li, Z.; Chen, P.; Huang, H.; Hurst, L.D.; Chen, J. Young Intragenic MiRNAs Are Less Coexpressed with Host Genes than Old Ones: Implications of MiRNA–Host Gene Coevolution. *Nucleic Acids Res.* **2012**, *40*, 4002–4012. [CrossRef] [PubMed]

32. Marsico, A.; Huska, M.R.; Lasserre, J.; Hu, H.; Vucicevic, D.; Musahl, A.; Orom, U.A.; Vingron, M. PROmiRNA: A New MiRNA Promoter Recognition Method Uncovers the Complex Regulation of Intronic MiRNAs. *Genome Biol.* **2013**, *14*, R84. [CrossRef] [PubMed]
33. Borchert, G.M.; Lanier, W.; Davidson, B.L. RNA Polymerase III Transcribes Human MicroRNAs. *Nat. Struct. Mol. Biol.* **2006**, *13*, 1097–1101. [CrossRef]
34. Diebel, K.W.; Smith, A.L.; van Dyk, L.F. Mature and Functional Viral MiRNAs Transcribed from Novel RNA Polymerase III Promoters. *RNA* **2010**, *16*, 170–185. [CrossRef] [PubMed]
35. Saini, H.K.; Griffiths-Jones, S.; Enright, A.J. Genomic Analysis of Human MicroRNA Transcripts. *Proc. Natl. Acad. Sci. USA* **2007**, *104*, 17719–17724. [CrossRef] [PubMed]
36. Altuvia, Y.; Landgraf, P.; Lithwick, G.; Elefant, N.; Pfeffer, S.; Aravin, A.; Brownstein, M.J.; Tuschl, T.; Margalit, H. Clustering and Conservation Patterns of Human MicroRNAs. *Nucleic Acids Res.* **2005**, *33*, 2697–2706. [CrossRef] [PubMed]
37. O'Brien, J.; Hayder, H.; Zayed, Y.; Peng, C. Overview of MicroRNA Biogenesis, Mechanisms of Actions, and Circulation. *Front. Endocrinol.* **2018**, *9*, 402. [CrossRef]
38. Ha, M.; Kim, V.N. Regulation of MicroRNA Biogenesis. *Nat. Rev. Mol. Cell Biol.* **2014**, *15*, 509–524. [CrossRef]
39. Roden, C.; Gaillard, J.; Kanoria, S.; Rennie, W.; Barish, S.; Cheng, J.; Pan, W.; Liu, J.; Cotsapas, C.; Ding, Y.; et al. Novel Determinants of Mammalian Primary MicroRNA Processing Revealed by Systematic Evaluation of Hairpin-Containing Transcripts and Human Genetic Variation. *Genome Res.* **2017**, *27*, 374–384. [CrossRef]
40. Yoshida, T.; Asano, Y.; Ui-Tei, K. Modulation of MicroRNA Processing by Dicer via Its Associated DsRNA Binding Proteins. *Non-Coding RNA* **2021**, *7*, 57. [CrossRef]
41. Sheng, P.; Fields, C.; Aadland, K.; Wei, T.; Kolaczkowski, O.; Gu, T.; Kolaczkowski, B.; Xie, M. Dicer Cleaves 5′-Extended MicroRNA Precursors Originating from RNA Polymerase II Transcription Start Sites. *Nucleic Acids Res.* **2018**, *46*, 5737–5752. [CrossRef] [PubMed]
42. Iwakawa, H.; Tomari, Y. Life of RISC: Formation, Action, and Degradation of RNA-Induced Silencing Complex. *Mol. Cell* **2022**, *82*, 30–43. [CrossRef] [PubMed]
43. Santhekadur, P.K.; Kumar, D.P. RISC Assembly and Post-Transcriptional Gene Regulation in Hepatocellular Carcinoma. *Genes Dis.* **2020**, *7*, 199–204. [CrossRef] [PubMed]
44. Dana, H.; Chalbatani, G.M.; Mahmoodzadeh, H.; Karimloo, R.; Rezaiean, O.; Moradzadeh, A.; Mehmandoost, N.; Moazzen, F.; Mazraeh, A.; Marmari, V.; et al. Molecular Mechanisms and Biological Functions of SiRNA. *Int. J. Biomed. Sci.* **2017**, *13*, 48–57.
45. Lambeth, L.S.; Smith, C.A. Short Hairpin RNA-Mediated Gene Silencing. In *Methods in Molecular Biology*; Clifton, N.J., Ed.; Humana Press: Totowa, NJ, USA, 2013; pp. 205–232; ISBN 978-1-62703-118-9.
46. Zhang, J.; Chen, S.; Liu, K. Structural Insights into PiRNA Biogenesis. *Biochim. Biophys. Acta Gene Regul. Mech.* **2022**, *1865*, 194799. [CrossRef]
47. Wu, J.; Yang, J.; Cho, W.C.; Zheng, Y. Argonaute Proteins: Structural Features, Functions and Emerging Roles. *J. Adv. Res.* **2020**, *24*, 317–324. [CrossRef]
48. Nakanishi, K. Anatomy of Four Human Argonaute Proteins. *Nucleic Acids Res.* **2022**, *50*, 6618–6638. [CrossRef]
49. Rouya, C.; Siddiqui, N.; Morita, M.; Duchaine, T.F.; Fabian, M.R.; Sonenberg, N. Human DDX6 Effects MiRNA-Mediated Gene Silencing via Direct Binding to CNOT1. *RNA* **2014**, *20*, 1398–1409. [CrossRef]
50. Hwang, H.-W.; Mendell, J.T. MicroRNAs in Cell Proliferation, Cell Death, and Tumorigenesis. *Br. J. Cancer* **2006**, *94*, 776–780. [CrossRef]
51. Esquela-Kerscher, A.; Slack, F.J. Oncomirs—MicroRNAs with a Role in Cancer. *Nat. Rev. Cancer* **2006**, *6*, 259–269. [CrossRef]
52. Fu, Z.; Wang, L.; Li, S.; Chen, F.; Au-Yeung, K.K.-W.; Shi, C. MicroRNA as an Important Target for Anticancer Drug Development. *Front. Pharmacol.* **2021**, *12*, 736323. [CrossRef]
53. Forterre, A.; Komuro, H.; Aminova, S.; Harada, M. A Comprehensive Review of Cancer MicroRNA Therapeutic Delivery Strategies. *Cancers* **2020**, *12*, 1852. [CrossRef] [PubMed]
54. Jansson, M.D.; Lund, A.H. MicroRNA and Cancer. *Mol. Oncol.* **2012**, *6*, 590–610. [CrossRef]
55. Zhang, X.; Dong, H.; Tian, Y. MiRNA Biology in Pathological Processes. In *MicroRNA Detection and Pathological Functions*; Springer : Berlin/Heidelberg, Germany, 2015; pp. 7–22; ISBN 978-3-662-47293-4.
56. Fuziwara, C.S.; Kimura, E.T. Insights into Regulation of the MiR-17-92 Cluster of MiRNAs in Cancer. *Front. Med.* **2015**, *2*, 64. [CrossRef] [PubMed]
57. Saiyed, A.N.; Vasavada, A.R.; Johar, S.R.K. Recent Trends in MiRNA Therapeutics and the Application of Plant MiRNA for Prevention and Treatment of Human Diseases. *Future J. Pharm. Sci.* **2022**, *8*, 24. [CrossRef]
58. He, B.; Zhao, Z.; Cai, Q.; Zhang, Y.; Zhang, P.; Shi, S.; Xie, H.; Peng, X.; Yin, W.; Tao, Y.; et al. MiRNA-Based Biomarkers, Therapies, and Resistance in Cancer. *Int. J. Biol. Sci.* **2020**, *16*, 2628–2647. [CrossRef]
59. Tagliaferri, P.; Rossi, M.; Di Martino, M.T.; Amodio, N.; Leone, E.; Gulla, A.; Neri, A.; Tassone, P. Promises and Challenges of MicroRNA-Based Treatment of Multiple Myeloma. *Curr. Cancer Drug Targets* **2012**, *12*, 838–846. [CrossRef] [PubMed]
60. De Jong, W.H.; Borm, P.J.A. Drug Delivery and Nanoparticles:Applications and Hazards. *Int. J. Nanomed.* **2008**, *3*, 133–149. [CrossRef] [PubMed]
61. Yue, J.; Feliciano, T.J.; Li, W.; Lee, A.; Odom, T.W. Gold Nanoparticle Size and Shape Effects on Cellular Uptake and Intracellular Distribution of SiRNA Nanoconstructs. *Bioconjug. Chem.* **2017**, *28*, 1791–1800. [CrossRef]

62. He, C.; Hu, Y.; Yin, L.; Tang, C.; Yin, C. Effects of Particle Size and Surface Charge on Cellular Uptake and Biodistribution of Polymeric Nanoparticles. *Biomaterials* **2010**, *31*, 3657–3666. [CrossRef]
63. Shang, L.; Nienhaus, K.; Nienhaus, G.U. Engineered Nanoparticles Interacting with Cells: Size Matters. *J. Nanobiotechnol.* **2014**, *12*, 5. [CrossRef] [PubMed]
64. Yameen, B.; Choi, W.I.; Vilos, C.; Swami, A.; Shi, J.; Farokhzad, O.C. Insight into Nanoparticle Cellular Uptake and Intracellular Targeting. *J. Control. Release* **2014**, *190*, 485–499. [CrossRef] [PubMed]
65. Fröhlich, E. The Role of Surface Charge in Cellular Uptake and Cytotoxicity of Medical Nanoparticles. *Int. J. Nanomed.* **2012**, *7*, 5577–5591. [CrossRef] [PubMed]
66. Noël, C.; Simard, J.-C.; Girard, D. Gold Nanoparticles Induce Apoptosis, Endoplasmic Reticulum Stress Events and Cleavage of Cytoskeletal Proteins in Human Neutrophils. *Toxicol. Vitr.* **2016**, *31*, 12–22. [CrossRef]
67. Chithrani, B.D.; Ghazani, A.A.; Chan, W.C.W. Determining the Size and Shape Dependence of Gold Nanoparticle Uptake into Mammalian Cells. *Nano Lett.* **2006**, *6*, 662–668. [CrossRef]
68. Nambara, K.; Niikura, K.; Mitomo, H.; Ninomiya, T.; Takeuchi, C.; Wei, J.; Matsuo, Y.; Ijiro, K. Reverse Size Dependences of the Cellular Uptake of Triangular and Spherical Gold Nanoparticles. *Langmuir* **2016**, *32*, 12559–12567. [CrossRef]
69. Xie, X.; Liao, J.; Shao, X.; Li, Q.; Lin, Y. The Effect of Shape on Cellular Uptake of Gold Nanoparticles in the Forms of Stars, Rods, and Triangles. *Sci. Rep.* **2017**, *7*, 3827. [CrossRef]
70. Kumal, R.R.; Landry, C.R.; Abu-Laban, M.; Hayes, D.J.; Haber, L.H. Monitoring the Photocleaving Dynamics of Colloidal MicroRNA-Functionalized Gold Nanoparticles Using Second Harmonic Generation. *Langmuir* **2015**, *31*, 9983–9990. [CrossRef]
71. Verderio, P.; Avvakumova, S.; Alessio, G.; Bellini, M.; Colombo, M.; Galbiati, E.; Mazzucchelli, S.; Avila, J.P.; Santini, B.; Prosperi, D. Delivering Colloidal Nanoparticles to Mammalian Cells: A Nano–Bio Interface Perspective. *Adv. Healthc. Mater.* **2014**, *3*, 957–976. [CrossRef]
72. Creusat, G.; Rinaldi, A.-S.; Weiss, E.; Elbaghdadi, R.; Remy, J.-S.; Mulherkar, R.; Zuber, G. Proton Sponge Trick for PH-Sensitive Disassembly of Polyethylenimine-Based SiRNA Delivery Systems. *Bioconjug. Chem.* **2010**, *21*, 994–1002. [CrossRef]
73. Guo, S.; Huang, L. Nanoparticles Escaping RES and Endosome: Challenges for SiRNA Delivery for Cancer Therapy. *J. Nanomater.* **2011**, *2011*, 742895. [CrossRef]
74. Ding, Y.; Jiang, Z.; Saha, K.; Kim, C.S.; Kim, S.T.; Landis, R.F.; Rotello, V.M. Gold Nanoparticles for Nucleic Acid Delivery. *Mol. Ther.* **2014**, *22*, 1075–1083. [CrossRef] [PubMed]
75. Nel, A.E.; Mädler, L.; Velegol, D.; Xia, T.; Hoek, E.M.V.; Somasundaran, P.; Klaessig, F.; Castranova, V.; Thompson, M. Understanding Biophysicochemical Interactions at the Nano–Bio Interface. *Nat. Mater.* **2009**, *8*, 543–557. [CrossRef] [PubMed]
76. Benjaminsen, R.V.; Mattebjerg, M.A.; Henriksen, J.R.; Moghimi, S.M.; Andresen, T.L. The Possible "Proton Sponge" Effect of Polyethylenimine (PEI) Does Not Include Change in Lysosomal PH. *Mol. Ther.* **2013**, *21*, 149–157. [CrossRef]
77. Freeman, E.C.; Weiland, L.M.; Meng, W.S. Modeling the Proton Sponge Hypothesis: Examining Proton Sponge Effectiveness for Enhancing Intracellular Gene Delivery through Multiscale Modeling. *J. Biomater. Sci. Polym. Ed.* **2013**, *24*, 398–416. [CrossRef] [PubMed]
78. Colangelo, E.; Comenge, J.; Paramelle, D.; Volk, M.; Chen, Q.; Lévy, R. Characterizing Self-Assembled Monolayers on Gold Nanoparticles. *Bioconjug. Chem.* **2017**, *28*, 11–22. [CrossRef] [PubMed]
79. Love, J.C.; Estroff, L.A.; Kriebel, J.K.; Nuzzo, R.G.; Whitesides, G.M. Self-Assembled Monolayers of Thiolates on Metals as a Form of Nanotechnology. *Chem. Rev.* **2005**, *105*, 1103–1170. [CrossRef] [PubMed]
80. Vakarelski, I.U.; McNamee, C.E.; Higashitani, K. Deposition of Silica Nanoparticles on a Gold Surface via a Self-Assembled Monolayer of (3-Mercaptopropyl)Trimethoxysilane. *Colloids Surf. A Physicochem. Eng. Asp.* **2007**, *295*, 16–20. [CrossRef]
81. Ahmed, S.R.; Oh, S.; Baba, R.; Zhou, H.; Hwang, S.; Lee, J.; Park, E.Y. Synthesis of Gold Nanoparticles with Buffer-Dependent Variations of Size and Morphology in Biological Buffers. *Nanoscale Res. Lett.* **2016**, *11*, 65. [CrossRef]
82. Heddle, J.G. Gold Nanoparticle-Biological Molecule Interactions and Catalysis. *Catalysts* **2013**, *3*, 683–708. [CrossRef]
83. Sperling, R.A.; García-Fernández, L.; Ojea-Jiménez, I.; Piella, J.; Bastús, N.G.; Puntes, V. One-Pot Synthesis of Cationic Gold Nanoparticles by Differential Reduction. *Z. Phys. Chem.* **2017**, *231*, 7–18. [CrossRef]
84. Vericat, C.; Vela, M.E.; Corthey, G.; Pensa, E.; Cortés, E.; Fonticelli, M.H.; Ibañez, F.; Benitez, G.E.; Carro, P.; Salvarezza, R.C. Self-Assembled Monolayers of Thiolates on Metals: A Review Article on Sulfur-Metal Chemistry and Surface Structures. *RSC Adv.* **2014**, *4*, 27730–27754. [CrossRef]
85. Smith, A.M.; Marbella, L.E.; Johnston, K.A.; Hartmann, M.J.; Crawford, S.E.; Kozycz, L.M.; Seferos, D.S.; Millstone, J.E. Quantitative Analysis of Thiolated Ligand Exchange on Gold Nanoparticles Monitored by 1H NMR Spectroscopy. *Anal. Chem.* **2015**, *87*, 2771–2778. [CrossRef]
86. Smith, A.M.; Millstone, J.E. Ligand Exchange and 1H NMR Quantification of Single- and Mixed-Moiety Thiolated Ligand Shells on Gold Nanoparticles. In *Biomedical Nanotechnology: Methods and Protocols*; Petrosko, S.H., Day, E.S., Eds.; Springer: New York, NY, USA, 2017; pp. 17–29; ISBN 978-1-4939-6840-4.
87. Chen, J.; Wu, Y.; Fu, C.; Cao, H.; Tan, X.; Shi, W.; Wu, Z. Ratiometric SERS Biosensor for Sensitive and Reproducible Detection of MicroRNA Based on Mismatched Catalytic Hairpin Assembly. *Biosens. Bioelectron.* **2019**, *143*, 111619. [CrossRef]
88. Wu, X.; Chai, Y.; Yuan, R.; Su, H.; Han, J. A Novel Label-Free Electrochemical MicroRNA Biosensor Using Pd Nanoparticles as Enhancer and Linker. *Analyst* **2013**, *138*, 1060–1066. [CrossRef]

89. Qing, Z.; Luo, G.; Xing, S.; Zou, Z.; Lei, Y.; Liu, J.; Yang, R. Pt–S Bond-Mediated Nanoflares for High-Fidelity Intracellular Applications by Avoiding Thiol Cleavage. *Angew. Chem. Int. Ed.* **2020**, *59*, 14044–14048. [CrossRef]
90. Huang, D.; Zhou, H.; Liu, H.; Gao, J. The Cytotoxicity of Gold Nanoparticles Is Dispersity-Dependent. *Dalton Trans.* **2015**, *44*, 17911–17915. [CrossRef]
91. Min, Y.; Akbulut, M.; Kristiansen, K.; Golan, Y.; Israelachvili, J. The Role of Interparticle and External Forces in Nanoparticle Assembly. *Nat. Mater.* **2008**, *7*, 527–538. [CrossRef]
92. Rosická, D.; Šembera, J. Changes in the Nanoparticle Aggregation Rate Due to the Additional Effect of Electrostatic and Magnetic Forces on Mass Transport Coefficients. *Nanoscale Res. Lett.* **2013**, *8*, 20. [CrossRef] [PubMed]
93. Gao, J.; Huang, X.; Liu, H.; Zan, F.; Ren, J. Colloidal Stability of Gold Nanoparticles Modified with Thiol Compounds: Bioconjugation and Application in Cancer Cell Imaging. *Langmuir* **2012**, *28*, 4464–4471. [CrossRef] [PubMed]
94. Yoon, J.; Shin, M.; Lee, J.-Y.; Lee, S.-N.; Choi, J.-H.; Choi, J.-W. RNA Interference (RNAi)-Based Plasmonic Nanomaterials for Cancer Diagnosis and Therapy. *J. Control. Release* **2022**, *342*, 228–240. [CrossRef] [PubMed]
95. Moraes, F.C.; Pichon, C.; Letourneur, D.; Chaubet, F. miRNA Delivery by Nanosystems: State of the Art and Perspectives. *Pharmaceutics* **2021**, *13*, 1901. [CrossRef] [PubMed]
96. Nahalka, J. The Role of the Protein–RNA Recognition Code in Neurodegeneration. *Cell. Mol. Life Sci.* **2019**, *76*, 2043–2058. [CrossRef] [PubMed]
97. Cristina Caroleo, M.; De Sarro, G. Chapter 24—Overview of MicroRNA-Based Therapeutics. In *MicroRNA*; Xiao, J., Ed.; Academic Press: Cambridge, MA, USA, 2022; pp. 493–502; ISBN 978-0-323-89774-7.
98. Muthiah, M.; Park, I.-K.; Cho, C.-S. Nanoparticle-Mediated Delivery of Therapeutic Genes: Focus on MiRNA Therapeutics. *Expert Opin. Drug Deliv.* **2013**, *10*, 1259–1273. [CrossRef] [PubMed]
99. Arghiani, N.; Shah, K. Modulating MicroRNAs in Cancer: Next-Generation Therapies. *Cancer Biol. Med.* **2022**, *19*, 289. [CrossRef] [PubMed]
100. Mansouri, S.; Lavigne, P.; Corsi, K.; Benderdour, M.; Beaumont, E.; Fernandes, J.C. Chitosan-DNA Nanoparticles as Non-Viral Vectors in Gene Therapy: Strategies to Improve Transfection Efficacy. *Eur. J. Pharm. Biopharm.* **2004**, *57*, 1–8. [CrossRef]
101. Thomas, T.J.; Tajmir-Riahi, H.A.; Pillai, C.K.S. Biodegradable Polymers for Gene Delivery. *Molecules* **2019**, *24*, 3744. [CrossRef]
102. Uchida, S.; Perche, F.; Pichon, C.; Cabral, H. Nanomedicine-Based Approaches for MRNA Delivery. *Mol. Pharm.* **2020**, *17*, 3654–3684. [CrossRef]
103. Chaudhari, R.; Nasra, S.; Meghani, N.; Kumar, A. MiR-206 Conjugated Gold Nanoparticle Based Targeted Therapy in Breast Cancer Cells. *Sci. Rep.* **2022**, *12*, 4713. [CrossRef]
104. Boca, S.; Gulei, D.; Zimta, A.-A.; Onaciu, A.; Magdo, L.; Tigu, A.B.; Ionescu, C.; Irimie, A.; Buiga, R.; Berindan-Neagoe, I. Nanoscale Delivery Systems for MicroRNAs in Cancer Therapy. *Cell. Mol. Life Sci.* **2020**, *77*, 1059–1086. [CrossRef]
105. Lee, S.W.L.; Paoletti, C.; Campisi, M.; Osaki, T.; Adriani, G.; Kamm, R.D.; Mattu, C.; Chiono, V. MicroRNA Delivery through Nanoparticles. *J. Control. Release* **2019**, *313*, 80–95. [CrossRef] [PubMed]
106. Hao, L.; Patel, P.C.; Alhasan, A.H.; Giljohann, D.A.; Mirkin, C.A. Nucleic Acid–Gold Nanoparticle Conjugates as Mimics of MicroRNA. *Small* **2011**, *7*, 3158–3162. [CrossRef] [PubMed]
107. Lin, L.; Fan, Y.; Gao, F.; Jin, L.; Li, D.; Sun, W.; Li, F.; Qin, P.; Shi, Q.; Shi, X.; et al. UTMD-Promoted Co-Delivery of Gemcitabine and MiR-21 Inhibitor by Dendrimer-Entrapped Gold Nanoparticles for Pancreatic Cancer Therapy. *Theranostics* **2018**, *8*, 1923–1939. [CrossRef] [PubMed]
108. Sun, T.; Simmons, R.; Huo, D.; Pang, B.; Zhao, X.; Kim, C.W.; Jo, H.; Xia, Y. Targeted Delivery of Anti-MiR-712 by VCAM1-Binding Au Nanospheres for Atherosclerosis Therapy. *ChemNanoMat* **2016**, *2*, 400–406. [CrossRef]
109. Natarajan, A.; Venugopal, S.K.; DeNardo, S.J.; Zern, M.A. Breast Cancer Targeting Novel MicroRNA-Nanoparticles for Imaging. In *Multimodal Biomedical Imaging IV*; SPIE: Washington, DC, USA, 2009; Volume 7171.
110. Kouri, F.M.; Hurley, L.A.; Daniel, W.L.; Day, E.S.; Hua, Y.; Hao, L.; Peng, C.-Y.; Merkel, T.J.; Queisser, M.A.; Ritner, C.; et al. MiR-182 Integrates Apoptosis, Growth, and Differentiation Programs in Glioblastoma. *Genes Dev.* **2015**, *29*, 732–745. [CrossRef]
111. Kim, J.-H.; Yeom, J.-H.; Ko, J.-J.; Han, M.S.; Lee, K.; Na, S.-Y.; Bae, J. Effective Delivery of Anti-MiRNA DNA Oligonucleotides by Functionalized Gold Nanoparticles. *J. Biotechnol.* **2011**, *155*, 287–292. [CrossRef]
112. van der Ven, C.F.T.; Tibbitt, M.W.; Conde, J.; van Mil, A.; Hjortnaes, J.; Doevendans, P.A.; Sluijter, J.P.G.; Aikawa, E.; Langer, R.S. Controlled Delivery of Gold Nanoparticle-Coupled MiRNA Therapeutics via an Injectable Self-Healing Hydrogel. *Nanoscale* **2021**, *13*, 20451–20461. [CrossRef]
113. Crew, E.; Rahman, S.; Razzak-Jaffar, A.; Mott, D.; Kamundi, M.; Yu, G.; Tchah, N.; Lee, J.; Bellavia, M.; Zhong, C.-J. MicroRNA Conjugated Gold Nanoparticles and Cell Transfection. *Anal. Chem.* **2012**, *84*, 26–29. [CrossRef]
114. Ghosh, R.; Singh, L.C.; Shohet, J.M.; Gunaratne, P.H. A Gold Nanoparticle Platform for the Delivery of Functional MicroRNAs into Cancer Cells. *Biomaterials* **2013**, *34*, 807–816. [CrossRef]
115. Ren, Y.; Wang, R.; Gao, L.; Li, K.; Zhou, X.; Guo, H.; Liu, C.; Han, D.; Tian, J.; Ye, Q.; et al. Sequential Co-Delivery of MiR-21 Inhibitor Followed by Burst Release Doxorubicin Using NIR-Responsive Hollow Gold Nanoparticle to Enhance Anticancer Efficacy. *J. Control. Release* **2016**, *228*, 74–86. [CrossRef]
116. Dang, M.N.; Gomez Casas, C.; Day, E.S. Photoresponsive MiR-34a/Nanoshell Conjugates Enable Light-Triggered Gene Regulation to Impair the Function of Triple-Negative Breast Cancer Cells. *Nano Lett.* **2021**, *21*, 68–76. [CrossRef] [PubMed]

117. Bao, S.; Huang, S.; Liu, Y.; Hu, Y.; Wang, W.; Ji, M.; Li, H.; Zhang, N.X.; Song, C.; Duan, S. Gold Nanocages with Dual Modality for Image-Guided Therapeutics. *Nanoscale* **2017**, *9*, 7284–7296. [CrossRef] [PubMed]
118. Huang, S.; Duan, S.; Wang, J.; Bao, S.; Qiu, X.; Li, C.; Liu, Y.; Yan, L.; Zhang, Z.; Hu, Y. Folic-Acid-Mediated Functionalized Gold Nanocages for Targeted Delivery of Anti-MiR-181b in Combination of Gene Therapy and Photothermal Therapy against Hepatocellular Carcinoma. *Adv. Funct. Mater.* **2016**, *26*, 2532–2544. [CrossRef]
119. Huang, S.; Liu, Y.; Xu, X.; Ji, M.; Li, Y.; Song, C.; Duan, S.; Hu, Y. Triple Therapy of Hepatocellular Carcinoma with MicroRNA-122 and Doxorubicin Co-Loaded Functionalized Gold Nanocages. *J. Mater. Chem. B* **2018**, *6*, 2217–2229. [CrossRef]
120. Sukumar, U.K.; Bose, R.J.C.; Malhotra, M.; Babikir, H.A.; Afjei, R.; Robinson, E.; Zeng, Y.; Chang, E.; Habte, F.; Sinclair, R.; et al. Intranasal Delivery of Targeted Polyfunctional Gold–Iron Oxide Nanoparticles Loaded with Therapeutic MicroRNAs for Combined Theranostic Multimodality Imaging and Presensitization of Glioblastoma to Temozolomide. *Biomaterials* **2019**, *218*, 119342. [CrossRef]
121. Mohammadniaei, M.; Lee, T.; Bharate, B.G.; Yoon, J.; Choi, H.K.; Park, S.; Kim, J.; Kim, J.; Choi, J.-W. Bifunctional Au@Bi_2Se_3 Core–Shell Nanoparticle for Synergetic Therapy by SERS-Traceable AntagomiR Delivery and Photothermal Treatment. *Small* **2018**, *14*, 1802934. [CrossRef]
122. Duff, D.G.; Baiker, A.; Edwards, P.P. A New Hydrosol of Gold Clusters. 1. Formation and Particle Size Variation. *Langmuir* **1993**, *9*, 2301–2309. [CrossRef]
123. Liu, R.; Wang, Q.; Li, Q.; Yang, X.; Wang, K.; Nie, W. Surface Plasmon Resonance Biosensor for Sensitive Detection of MicroRNA and Cancer Cell Using Multiple Signal Amplification Strategy. *Biosens. Bioelectron.* **2017**, *87*, 433–438. [CrossRef]
124. Huang, J.; Shangguan, J.; Guo, Q.; Ma, W.; Wang, H.; Jia, R.; Ye, Z.; He, X.; Wang, K. Colorimetric and Fluorescent Dual-Mode Detection of MicroRNA Based on Duplex-Specific Nuclease Assisted Gold Nanoparticle Amplification. *Analyst* **2019**, *144*, 4917–4924. [CrossRef]
125. Yu, S.; Wang, Y.; Jiang, L.-P.; Bi, S.; Zhu, J.-J. Cascade Amplification-Mediated In Situ Hot-Spot Assembly for MicroRNA Detection and Molecular Logic Gate Operations. *Anal. Chem.* **2018**, *90*, 4544–4551. [CrossRef]
126. Esmaeili-bandboni, A.; Amini, S.M.; Faridi-majidi, R.; Bagheri, J.; Mohammadnejad, J.; Sadroddiny, E. Cross-Linking Gold Nanoparticles Aggregation Method Based on Localised Surface Plasmon Resonance for Quantitative Detection of MiR-155. *IET Nanobiotechnol.* **2018**, *12*, 453–458. [CrossRef]
127. Cai, J.; Ding, L.; Gong, P.; Huang, J. A Colorimetric Detection of MicroRNA-148a in Gastric Cancer by Gold Nanoparticle–RNA Conjugates. *Nanotechnology* **2019**, *31*, 095501. [CrossRef] [PubMed]
128. Mollasalehi, H.; Shajari, E. A Colorimetric Nano-Biosensor for Simultaneous Detection of Prevalent Cancers Using Unamplified Cell-Free Ribonucleic Acid Biomarkers. *Bioorg. Chem.* **2021**, *107*, 104605. [CrossRef] [PubMed]
129. Li, J.; Huang, J.; Yang, X.; Yang, Y.; Quan, K.; Xie, N.; Wu, Y.; Ma, C.; Wang, K. Two-Color-Based Nanoflares for Multiplexed MicroRNAs Imaging in Live Cells. *Nanotheranostics* **2018**, *2*, 96–105. [CrossRef]
130. Zhao, J.; Liu, C.; Li, Y.; Ma, Y.; Deng, J.; Li, L.; Sun, J. Thermophoretic Detection of Exosomal MicroRNAs by Nanoflares. *J. Am. Chem. Soc.* **2020**, *142*, 4996–5001. [CrossRef]
131. Hwu, S.; Blickenstorfer, Y.; Tiefenauer, R.F.; Gonnelli, C.; Schmidheini, L.; Lüchtefeld, I.; Hoogenberg, B.-J.; Gisiger, A.B.; Vörös, J. Dark-Field Microwells toward High-Throughput Direct MiRNA Sensing with Gold Nanoparticles. *ACS Sens.* **2019**, *4*, 1950–1956. [CrossRef] [PubMed]
132. Canady, T.D.; Li, N.; Smith, L.D.; Lu, Y.; Kohli, M.; Smith, A.M.; Cunningham, B.T. Digital-Resolution Detection of MicroRNA with Single-Base Selectivity by Photonic Resonator Absorption Microscopy. *Proc. Natl. Acad. Sci. USA* **2019**, *116*, 19362–19367. [CrossRef]
133. Peng, M.; Sun, F.; Na, N.; Ouyang, J. Target-Triggered Assembly of Nanogap Antennas to Enhance the Fluorescence of Single Molecules and Their Application in MicroRNA Detection. *Small* **2020**, *16*, 2000460. [CrossRef] [PubMed]
134. Qu, A.; Sun, M.; Xu, L.; Hao, C.; Wu, X.; Xu, C.; Kotov, N.A.; Kuang, H. Quantitative Zeptomolar Imaging of MiRNA Cancer Markers with Nanoparticle Assemblies. *Proc. Natl. Acad. Sci. USA* **2019**, *116*, 3391–3400. [CrossRef]
135. Zhang, L.; Wang, J.; Zhang, J.; Liu, Y.; Wu, L.; Shen, J.; Zhang, Y.; Hu, Y.; Fan, Q.; Huang, W.; et al. Individual Au-Nanocube Based Plasmonic Nanoprobe for Cancer Relevant MicroRNA Biomarker Detection. *ACS Sens.* **2017**, *2*, 1435–1440. [CrossRef]
136. Slabý, J.; Bocková, M.; Homola, J. Plasmonic Biosensor Based on a Gold Nanostripe Array for Detection of MicroRNA Related to Myelodysplastic Syndromes. *Sens. Actuators B Chem.* **2021**, *347*, 130629. [CrossRef]
137. Kim, W.H.; Lee, J.U.; Song, S.; Kim, S.; Choi, Y.J.; Sim, S.J. A Label-Free, Ultra-Highly Sensitive and Multiplexed SERS Nanoplasmonic Biosensor for MiRNA Detection Using a Head-Flocked Gold Nanopillar. *Analyst* **2019**, *144*, 1768–1776. [CrossRef] [PubMed]
138. Zhu, W.-F.; Cheng, L.-X.; Li, M.; Zuo, D.; Zhang, N.; Zhuang, H.-J.; Xie, D.; Zeng, Q.-D.; Hutchison, J.A.; Zhao, Y.-L. Frequency Shift Raman-Based Sensing of Serum MicroRNAs for Early Diagnosis and Discrimination of Primary Liver Cancers. *Anal. Chem.* **2018**, *90*, 10144–10151. [CrossRef] [PubMed]
139. Nie, W.; Wang, Q.; Yang, X.; Zhang, H.; Li, Z.; Gao, L.; Zheng, Y.; Liu, X.; Wang, K. High Sensitivity Surface Plasmon Resonance Biosensor for Detection of MicroRNA Based on Gold Nanoparticles-Decorated Molybdenum Sulfide. *Anal. Chim. Acta* **2017**, *993*, 55–62. [CrossRef]
140. Wang, Q.; Li, Q.; Yang, X.; Wang, K.; Du, S.; Zhang, H.; Nie, Y. Graphene Oxide–Gold Nanoparticles Hybrids-Based Surface Plasmon Resonance for Sensitive Detection of MicroRNA. *Biosens. Bioelectron.* **2016**, *77*, 1001–1007. [CrossRef]

141. Che, C.; Xue, R.; Li, N.; Gupta, P.; Wang, X.; Zhao, B.; Singamaneni, S.; Nie, S.; Cunningham, B.T. Accelerated Digital Biodetection Using Magneto-Plasmonic Nanoparticle-Coupled Photonic Resonator Absorption Microscopy. *ACS Nano* **2022**, *16*, 2345–2354. [CrossRef]
142. Islam, M.N.; Masud, M.K.; Nguyen, N.T.; Gopalan, V.; Alamri, H.R.; Alothman, Z.A.; Al Hossain, M.S.; Yamauchi, Y.; Lamd, A.K.; Shiddiky, M.J. Gold-Loaded Nanoporous Ferric Oxide Nanocubes for Electrocatalytic Detection of MicroRNA at Attomolar Level. *Biosens. Bioelectron.* **2018**, *101*, 275–281. [CrossRef]
143. Lee, J.-H.; Choi, J.-H.; Chueng, S.-T.D.; Pongkulapa, T.; Yang, L.; Cho, H.-Y.; Choi, J.-W.; Lee, K.-B. Nondestructive Characterization of Stem Cell Neurogenesis by a Magneto-Plasmonic Nanomaterial-Based Exosomal MiRNA Detection. *ACS Nano* **2019**, *13*, 8793–8803. [CrossRef]